Version 4.0
June 1996

Wide Field and Planetary Camera 2 Instrument Handbook

SPACE TELESCOPE SCIENCE INSTITUTE

Operated by the Association of Universities for Research in Astronomy, Inc., for the National Aeronautics and Space Administration

User Support

For prompt answers to questions, please contact the Science Support Division Help Desk.

- **E-mail:** help@stsci.edu
- **Phone:** (410) 338-1082

World Wide Web

Information, software tools, and other resources are available on the WFPC2 World Wide Web page:

- **URL:** `http://www.stsci.edu/ftp/instrument_news/WFPC2/top_wfpc2.html`

WFPC2 Instrument Team

Name	Title	Phone	e-mail
Brad Whitmore	Group Lead	410-338-4743	whitmore@stsci.edu
John Biretta	Technical Lead Scientist	410-338-4917	biretta@stsci.edu
Stefano Casertano	Calibration Lead Scientist	410-338-4752	stefano@stsci.edu
Keith Noll	User Support Lead Scientist	410-338-1828	noll@stsci.edu
Sylvia Baggett	Cal. Pipeline Lead Scientist	410-338-5054	sbaggett@stsci.edu
Harry Ferguson	Instrument Scientist	410-338-5098	ferguson@stsci.edu
Andrew Fruchter	Instrument Scientist	410-338-5018	fruchter@stsci.edu
Christopher O'Dea	Instrument Scientist	410-338-2590	odea@stsci.edu
Massimo Stiavelli	Instrument Scientist	410-338-4835	mstiavel@stsci.edu
Anatoly Suchkov	Instrument Scientist	410-338-4979	suchkov@stsci.edu
Jean Surdej	Instrument Scientist	410-338-4984	surdej@stsci.edu
Shireen Gonzaga	Data Analyst	410-338-4412	gonzaga@stsci.edu
Inge Heyer	Data Analyst	410-338-5017	heyer@stsci.edu
Matt McMaster	Data Analyst	410-338-4463	mcmaster@stsci.edu
Michael S. Wiggs	Data Analyst	410-338-4998	wiggs@stsci.edu
J.-C. Hsu	Scientific Programmer	410-338-4760	hsu@stsci.edu

The WFPC2 Investigation Definition Team:

John T. Trauger, Christopher J. Burrows, John Clarke, David Crisp, John Gallagher, Richard E. Griffiths, J. Jeff Hester, John Hoessel, Jon Holtzman, Jeremy Mould, and James A. Westphal

Handbook Authors and Contributors:

John Biretta, Chris Burrows, Jon Holtzman, Inge Heyer, Mark Stevens, Sylvia Baggett, Stefano Casertano, Mark Clampin, Andrew Fruchter, Harry Ferguson, Ron Gilliland, Richard Griffiths, John Krist, Keith Noll, Christopher O'Dea, Massimo Stiavelli, Anatoly Suchkov, Jean Surdej, and Brad Whitmore

Revision History

Instrument	Version	Date	Editor
WF/PC-1	1.0; 2.0; 2.1	October 1985; May 1989; May 1990	Richard Griffiths
WF/PC-1	3.0	April 1992	John W. MacKenty
WFPC2	1.0; 2.0; 3.0	March 1993; May 1994; June 1995	Christopher J. Burrows
WFPC2	4.0	June 1996	John A. Biretta

In publications please refer to this document as "Biretta, J. A., et al. 1996, WFPC2 Instrument Handbook, Version 4.0 (Baltimore: STScI)."

Table of Contents

CHAPTER 1: Introduction 1

Instrument Overview 1

Field-of-View 1
Spectral Filters 2
Quantum Efficiency and Exposure Limits 3
CCD Detector Technology 3
UV Imaging 4
Aberration Correction and Optical Alignment 5

Which Instrument to Use: WFPC2, FOC, NICMOS, or STIS? 6

Comparison of WFPC2 and FOC 6
Comparison of WFPC2 and NICMOS 8
Comparison of WFPC2 and STIS 10

History of WFPC2 11
The Previous vs. Current Generation: WF/PC-1 vs. WFPC2 13
Organization of this Handbook 15
What's New in Version 4.0 15
WFPC2 Handbook on the WWW 16
The Help Desk at STScI 16
Further Information 17

CHAPTER 2: Instrument Description 19

Science Objectives 19
WFPC2 Configuration, Field-of-View, and Resolution 20
Overall Instrument Description 21
Quantum Efficiency 24
Shutter 26
Serial Clocks 27
Overhead Times 29

CCD Orientation and Readout 31
Calibration Channel 33
CHAPTER 3: Optical Filters 35
Introduction 35
Choice of Broad Band Filters 40
Linear Ramp Filters 40
Spectral Response 40
Target Locations 45
LRF Photometric Calibration 45
Redshifted [OII] Quad Filters 49
Polarizer Quad Filter 50
Methane Quad Filter 53
Wood's Filters 54
Red Leaks in UV Filters 57
Apertures 60
CHAPTER 4: CCD Performance 63
Introduction 63
Quantum Efficiency 64
Dynamic Range 65
Bright Object Artifacts 66
Blooming 66
Horizontal Smearing 67
Diffraction Effects and Ghost Images 68
Residual Image 68
Quantum Efficiency Hysteresis 70
Flat Field Response 70
Dark Backgrounds 71
Sources of Dark Current 72
Darktime 73
Cosmic Rays 75
Radiation Damage and Hot Pixels 79
Charge Transfer Efficiency 80
Read Noise and Gain Settings 82

CHAPTER 5: Point Spread Function 85
Effects of OTA Spherical Aberration 85
Aberration Correction 86
Wavefront Quality 90
CCD Pixel Response Function 91
Model PSFs 92
PSF Variations with Field Position 95
PSF Variations with Time 97
Large Angle Scattering 99
Ghost Images 100
Optical Distortion 103
CHAPTER 6: System Throughput and SNR / Exposure Time Estimation 107
System Throughput 107
On-Line Exposure Time Calculator 110
Target Count Rates 111
Count Rates for Stellar Sources 111
Count Rates for Power Law Sources 112
Count Rates for Emission Line Sources 112
Sky Background 113
Signal-to-Noise Ratio Estimation 115
Point Sources -- PSF Fitting 115
Point Sources -- Aperture Photometry 118
Extended Sources 119
Exposure Time Estimation 122
Sample SNR Calculations 123
Point Sources 123
Extended Sources 129
Emission Line Sources 129
Red Leaks in UV Filters 137
Time Dependence of UV Response 137
CHAPTER 7: Observation Strategies 143
Observing Faint Targets 143

Observing Bright Targets ... 144
Observing Faint Targets Near Bright Objects ... 146
Cosmic Rays ... 151
Choosing Exposure Times ... 152
Dither Strategies ... 155
Pointing Accuracy ... 157
Absolute Pointing Accuracy ... 157
Updates to Aperture / Coordinate Systems ... 158
Pointing Repeatability ... 159
Tracking Modes ... 159
CCD Position and Orientation on Sky ... 159
Polarization Observations ... 162
Observing with Linear Ramp Filters ... 165
Emission Line Observations of Galaxy Nuclei ... 166
CHAPTER 8: Calibration and Data Reduction ... 167
Calibration Observations and Reference Data ... 167
Flat Fields ... 168
Dark Frames ... 169
Bias Frames ... 169
Data Reduction and Data Products ... 170
Pipeline Processing ... 170
Fluxes and Standard Magnitudes ... 171
Color Transformations - Primary Photometric Filters 172
Cycle 5 Calibration Plan ... 175
Cycle 6 Calibration Plan ... 185
CHAPTER 9: References ... 197
References ... 197
Instrument Science Reports ... 199
APPENDIX A: Passband Plots ... 201
Passbands for each Filter in Isolation ... 201
Passbands including the System Response ... 211

Normalized Passbands including the System Response 221
APPENDIX B: Point Source SNR Plots ... 223
Plots for Estimating Point Source SNR 223
APPENDIX C: Acronyms 239
INDEX 241

List of Figures

Figure 1.1: WFPC2 Field-of-View Projected on the Sky 2
Figure 2.1: Wide Field Planetary Camera Concept Illustration.................................... 21
Figure 2.2: WFPC2 Optical Configuration 22
Figure 2.3: Cooled Sensor Assembly.. 24
Figure 2.4: WFPC2 + OTA System Throughput.. 25
Figure 3.1: Summary of Normalized Filter Curves 39
Figure 3.2: Ramp Filter Peak Transmission 42
Figure 3.3: Ramp Filter Dimensionless Widths 42
Figure 3.4: FR418N and FR533N Wavelength Mapping... 46
Figure 3.5: FR680N and FR868N Wavelength Mapping... 47
Figure 3.6: Polarizer Quads... 52
Figure 3.7: Polarizer Transmission.. 53
Figure 3.8: Methane Quad Filter.. 55
Figure 3.9: Wood's Filters.. 56
Figure 3.10: UV Filter Red Leaks 58
Figure 3.11: Precise CCD Alignments and Primary Aperture Locations 62
Figure 4.1: MPP Operating Principle... 64
Figure 4.2: Pre-flight DQE Measurements on WFPC2 CCDs 66
Figure 4.3: Saturated Stellar Image Showing Horizontal Smearing 69
Figure 4.4: WFPC2 CCD Flat Field 71
Figure 4.5: Average Dark Rates vs. CCD Row 72
Figure 4.6: Dark Signal vs. Cosmic Ray Flux.. 74
Figure 4.7: Histogram of Cosmic Ray Event Sizes.. 76
Figure 4.8: Comparison of Star Images and Cosmic Ray Events 77
Figure 4.9: Histogram of Cosmic Ray Event Energies 78
Figure 4.10: Hot Pixel Histogram... 80
Figure 4.11: Images Illustrating CTE Residual Trail 83
Figure 5.1: PSF Surface Brightness.. 86
Figure 5.2: Encircled Energy 87
Figure 5.3: Encircled Energy for CCD PC1 88
Figure 5.4: Encircled Energy for CCD WF3... 89
Figure 5.5: PSF Variations with Field Position - Aberrations....................................... 95
Figure 5.6: PSF Variations with Field Position - Obscuration Shifts............................ 96
Figure 5.7: Measured OTA Focus Position (microns) vs. Time................................... 97
Figure 5.8: Measured Aperture Correction, V(r) - V(r=10 pix) 98
Figure 5.9: Large Angle Scattering.. 100

Figure 5.10: Saturated Stellar Image Showing Filter Ghosts 101
Figure 5.11: Saturated Stellar Image Showing Field Flattener Ghost on WF2........... 102
Figure 5.12: Integrated Photometry Correction Induced by Camera Distortions........ 105
Figure 6.1: Giant Elliptical Galaxy 122
Figure 6.2: Sample Fill-out Form for WFPC2 On-Line Exposure Time Calculator..... 126
Figure 6.3: Sample Results from WFPC2 ETC - Point Source 127
Figure 6.4: Sample Results on CR-SPLITing from WFPC2 ETC 127
Figure 6.5: Point Source + Stellar Background Fill-out Form for WFPC2 ETC 130
Figure 6.6: Sample Output from WFPC2 ETC - Point Source + Background 131
Figure 6.7: Extended Source Form for WFPC2 ETC 133
Figure 6.8: Sample Output from WFPC2 ETC - Extended Source............................ 134
Figure 6.9: Point Source Form for WFPC2 ETC - Emission Line & LRF.................... 136
Figure 6.10: Sample Output for WFPC2 ETC - Emission Line & LRF........................ 137
Figure 6.11: Photometric Monitoring Data for WFPC2 140
Figure 6.12: Throughput for the F170W Filter Following Decontaminations 141
Figure 6.13: Change in Throughput vs. Time 141
Figure 7.1: Example of Scattered Earth Light.. 145
Figure 7.2: Impact of OTA Focus Shift on PSF Subtraction 148
Figure 7.3: Bright Object Avoidance Regions Near WFPC2 FOV.............................. 149
Figure 7.4: Example of PC1 “Direct” Stray Light Ghost... 150
Figure 7.5: Example of PC1 “Diffraction” Stray Light Ghost 151
Figure 7.6: Event Timings During a 60s WFPC2 Exposure 153
Figure 7.7: Event Timings During a 100s WFPC2 Exposure 153
Figure 7.8: ORIENT Definition, Aperture Positions, and CCD Alignments................. 161
Figure 7.9: Example of ORIENT and POS TARG Selection 163
Figure 7.10: Example of ORIENT and POS TARG Selection 164
Figure 8.1: F336W-F439W against Johnson U-B... 173
Figure 8.2: F439W-F555W against Johnson B-V... 173
Figure 8.3: F555W-F814W against Johnson V-I_C 174
Figure 8.4: F555W-F675W against Johnson V-R_C... 174
Figure 8.5: F675W-F814W against Cousins R_C-I_C 175
Figure B.1: Point Source SNR vs. V+$AB_ν$ for F160BW Filter 225
Figure B.2: Point Source SNR vs. V+$AB_ν$ for F218W Filter....................................... 226
Figure B.3: Point Source SNR vs. V+$AB_ν$ for F255W Filter....................................... 227
Figure B.4: Point Source SNR vs. V+$AB_ν$ for F300W Filter....................................... 228
Figure B.5: Point Source SNR vs. V+$AB_ν$ for F336W Filter....................................... 229
Figure B.6: Point Source SNR vs. V+$AB_ν$ for F410M Filter 230
Figure B.7: Point Source SNR vs. V+$AB_ν$ for F439W Filter....................................... 231
Figure B.8: Point Source SNR vs. V+$AB_ν$ for F502N Filter.. 232
Figure B.9: Point Source SNR vs. V+$AB_ν$ for F547M Filter 233
Figure B.10: Point Source SNR vs. V+$AB_ν$ for F555W Filter..................................... 234

Figure B.11: Point Source SNR vs. V+AB_ν for F606W Filter 235
Figure B.12: Point Source SNR vs. V+AB_ν for F675W Filter 236
Figure B.13: Point Source SNR vs. V+AB_ν for F702W Filter 237
Figure B.14: Point Source SNR vs. V+AB_ν for F814W Filter 238

List of Tables

Table 1.1: Comparison of WFPC2, FOC, NICMOS, and STISI 6
Table 1.2: Comparison of WFPC2 and FOC Detective Efficiencies........... 7
Table 1.3: Comparison of WFPC2 and NICMOS Count Rates.................. 9
Table 1.4: Comparison of WFPC2 and STIS Detective Efficiencies 11
Table 2.1: Summary of Camera Format.. 20
Table 2.2: WFPC2 Dynamic Range in a Single Exposure 26
Table 2.3: Quantized Exposure Times (Seconds).................................... 27
Table 2.4: Instrument Overheads.. 31
Table 2.5: Inner Field Edges 31
Table 3.1: WFPC2 Simple Filter Set 37
Table 3.2: WFPC2 Quad and Ramp Filters... 38
Table 3.3: Ramp Filter FR418N Parameters.. 43
Table 3.4: Ramp Filter FR533N Parameters.. 43
Table 3.5: Ramp Filter FR680N Parameters.. 44
Table 3.6: Ramp Filter FR868N Parameters.. 44
Table 3.7: Aperture Locations and Wavelengths for Ramp Filters........... 48
Table 3.8: Vignetted Wavelengths for Ramp Filters................................. 49
Table 3.9: Redshifted [OII] Quad Filter Elements.................................... 50
Table 3.10: Polarizer Quad Filter 51
Table 3.11: Methane Band Quad Filter 54
Table 3.12: Wood's Filters... 57
Table 3.13: Red Leak in UV Filters 59
Table 3.14: Aperture Definitions.. 61
Table 3.15: Updates to (V2,V3) Positions of WFPC2 Apertures.............. 61
Table 4.1: Comparison of WF/PC-1 and WFPC2 CCDs.......................... 65
Table 4.2: Dark Count Rates... 73
Table 4.3: Signal Chain Gains... 82
Table 5.1: Wavefront Error Budget.. 87
Table 5.2: Aberrations in Each Camera 91
Table 5.3: PC Point Spread Functions.. 93
Table 5.4: WFC Point Spread Functions.. 94
Table 5.5: Cubic Distortion Coefficients 104
Table 6.1: System Efficiencies and Zeropoints 109
Table 6.2: AB_{ν} as a Function of Wavelength 110
Table 6.3: Sky Brightness 113
Table 6.4: Sky Count Rate per Pixel (Psky) 114

Table 6.5: Sharpness 116
Table 6.6: Parameters for Pt. Source SNR Est. - PSF Fitting 118
Table 6.7: Encircled Energy for Representative Filters 119
Table 6.8: Parameters for Pt. Source SNR Est. - Aperture Photom....... 119
Table 6.9: Parameters for Extended Source SNR Estimation................ 121
Table 6.10: Change in WFPC2 Throughput Over 30 Days 138
Table 7.1: ORIENTs for Avoiding Bloom and Diffraction Spikes............ 146
Table 7.2: Approx. PSF Subtraction Artifact Magnitudes 147
Table 7.3: Recommended Exposure Splittings 152
Table 7.4: Basic Time to Execute Single Non-CR-SPLIT Exposure 154
Table 8.1: Conversion from STMAG to UBVRI and Cousins RI............. 172
Table 8.2: Summary of Cycle 5 Calibration Plans.................................. 177
Table 8.3: Summary of Cycle 6 Calibration Plans.................................. 186
Table B.1: AB_ν as a Function of Wavelength 224
Table C.1: Acronyms.. 239

CHAPTER 1: Introduction

In This Chapter...

Instrument Overview / 1
Which Instrument to Use: WFPC2, FOC, NICMOS, or STIS? / 6
History of WFPC2 / 11
The Previous vs. Current Generation: WF/PC-1 vs. WFPC2 / 13
Organization of this Handbook / 15
What's New in Version 4.0 / 15
WFPC2 Handbook on the WWW / 16
The Help Desk at STScI / 16
Further Information / 17

1.1 Instrument Overview

Wide Field and Planetary Camera 2 (WFPC2) is a two-dimensional imaging photometer which is located at the center of the Hubble Space Telescope (HST) focal plane and covers the spectral range between approximately 1150Å to 10500Å. It simultaneously images a 150″ x 150″ "L"-shaped region with a spatial sampling of 0.1″ per pixel, and a smaller 34″ x 34″ square field with 0.046″ per pixel. The total system quantum efficiency (WFPC2+HST) ranges from 5% to 13% at visual wavelengths, and drops to ~0.5% in the far UV. Detection of faint targets will be limited by either the sky background (for broad filters) or by noise in the read-out electronics (for narrow and UV filters) with an RMS equivalent to 5 detected photons. Bright targets can cause saturation (>53000 detected photons per pixel), but there are no related safety issues. The sections below give a more detailed overview.

1.1.1 Field-of-View

The WFPC2 field-of-view is divided into four cameras by a four-faceted pyramid mirror near the HST focal plane. Each of the four cameras contains an 800x800 pixel Loral CCD detector. Three cameras operate at an image scale of 0.1″ per pixel (F/12.9) and comprise the Wide Field Camera (WFC) with an "L" shaped field-of-view. The fourth camera operates at 0.046″ per pixel (F/28.3) and is referred to as the Planetary Camera (PC). There are thus four sets of relay optics and CCD sensors in WFPC2. The four cameras are called PC1, WF2, WF3, and WF4, and their fields-of-view are illustrated in Figure 1.1 (see also "CCD Position and Orientation on Sky" on page 159). Each image is a mosaic of three F/12.9 images and one F/28.3 image.

Figure 1.1: WFPC2 Field-of-View Projected on the Sky. The readout direction is marked with arrows near the start of the first row in each CCD. The X-Y coordinate directions are for POS-TARG commands. The position angle of V3 varies with pointing direction and observation epoch, and is given in the calibrated science header by keyword PA_V3.

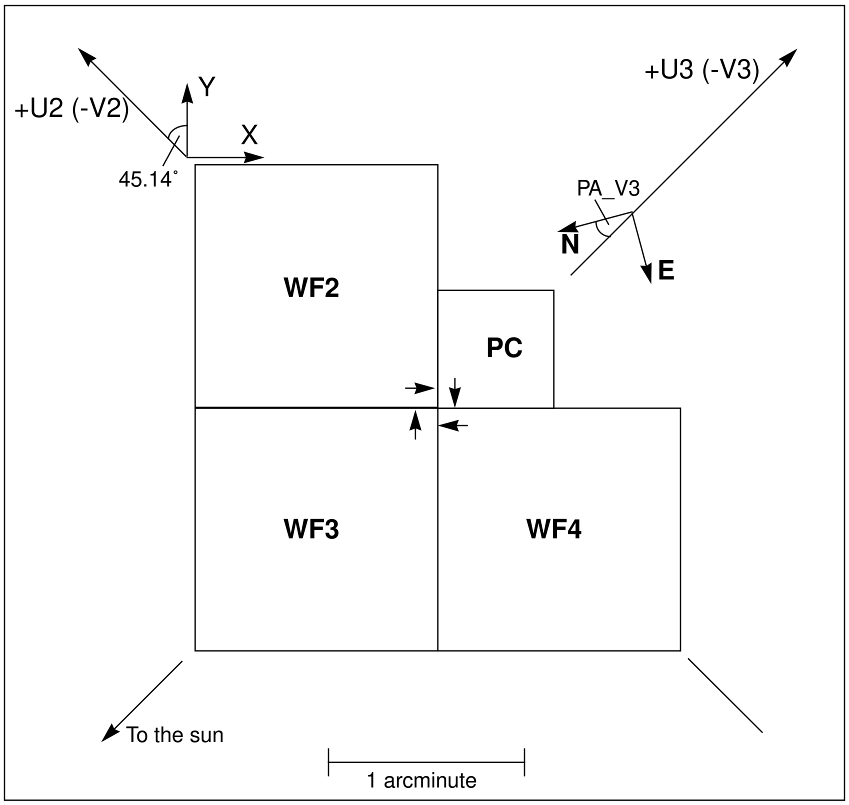

1.1.2 Spectral Filters

The WFPC2 contains 48 filters mounted in 12 wheels of the Selectable Optical Filter Assembly (SOFA). These include a set of broad band filters approximating Johnson-Cousins UBVRI, as well as a set of wide U, B, V, and R filters, and a set of medium bandwidth Strömgren *u, v*, *b*, and *y* filters.

Narrow band filters include those for emission lines of Ne V (3426Å), CN (~3900Å), [OIII] (4363Å and 5007Å), He II (4686Å), Hβ (4861Å), He I (5876Å), [OI] (6300Å), Hα (6563Å), [NII] (6583Å), [SII] (6716Å and 6731Å), and [SIII] (9531Å). The narrow-band filters are designed to have the same dimensionless bandpass profile. Center wavelengths and profiles are uniformly accurate over the filter clear apertures, and laboratory calibrations include profiles, blocking, and temperature shift coefficients.

There are also two narrow band "quad" filters, each containing four separate filters which image a limited field-of-view: the UV quad contains filters for observing redshifted [OII] emission and are centered at 3767Å, 3831Å, 3915Å, and 3993Å. The Methane quad contains filters at 5433Å, 6193Å, 7274Å, and 8929Å. Finally, there is a set of narrow band "linear ramp filters" (LRFs) which are continuously tunable from 3170Å to 9762Å; these provide a limited field-of-view with diameter ~10″.

At ultraviolet wavelengths there is a solar-blind Wood's UV filter (1200-1900Å). The UV capability is also enhanced by control of UV absorbing molecular contamination, the capability to remove UV absorbing accumulations on cold CCD windows without disrupting the CCD quantum efficiencies and flat field calibrations, and an internal source of UV reference flat field images.

Finally, there is a set of four polarizers set at four different angles, which can be used in conjunction with other filters for polarimetric measurements. However, due to the relatively high instrumental polarization of WFPC2, they are probably suitable only for measurements on strongly polarized sources (>3% polarized).

1.1.3 Quantum Efficiency and Exposure Limits

The quantum efficiency (QE) of WFPC2+HST peaks at 13% in the red, and remains above 5% over the visible spectrum. The UV response extends to Lyman α wavelengths (QE~0.5%). Internal optics provide spherical aberration correction.

Exposures of bright targets are limited by saturation effects, which appear above ~53000 detected photons per pixel (for setting ATD-GAIN=15), and by the shortest exposure time which is 0.11 seconds. There are no instrument safety issues associated with bright targets. Detection of faint targets is limited by the sky background for broad band filters at visual wavelengths. For narrow band and ultraviolet filters, detections are limited by noise in the read-out amplifier ("read noise"), which contributes an RMS noise equivalent to ~5 detected photons per pixel.

1.1.4 CCD Detector Technology

The WFPC2 CCDs are thick, front-side illuminated devices made by Loral. They support multi-pinned phase (MPP) operation which eliminates quantum efficiency hysteresis. They have a Lumogen phosphor coating to give UV sensitivity. Details may be summarized as follows:

- **Read noise:** WFPC2 CCDs have ~5e^- RMS read noise which provides good faint object and UV imaging capabilities.

- **Dark noise:** Inverted phase operation yields low dark noise for WFPC2 CCDs. They are being operated at -88˚C and the median dark current is about 0.0045 $e^- pixel^{-1} s^{-1}$.
- **Flat field:** WFPC2 CCDs have a uniform pixel-to-pixel response (<2% pixel-to-pixel non-uniformity) which facilitates accurate photometric calibration.
- **CTE:** Low level charge traps are present in the WFPC2 devices at the present operating temperature of -88˚C. On low background star fields, the traps result in a loss of about 4% of the signal when a star image is clocked down through all rows of the CCD. In the presence of background, the effect is reduced. For most applications, CTE is negligible or calibratable and pre-flash exposures are not required. This avoids the increase in background noise, and the decrease in operational efficiency that results from a preflash.
- **Gain switch:** Two CCD gains are available with WFPC2, a 7 $e^- DN^{-1}$ channel which saturates at about 27000 e^- (4096 DN with a bias of about 300 DN) and a 14 $e^- DN^{-1}$ channel which saturates at about 53000 e^-. The Loral devices have a full well capacity of ~90,000 e^- and are linear up to 4096 DN in both channels.
- **DQE:** The peak CCD DQE in the optical is 40% at 7000Å. In the UV (1100-4000Å) the DQE is determined by the phosphorescent Lumogen coating, and is 10 - 15%.
- **Image Purge:** The residual image resulting from a 100x (or more) full-well over-exposure is well below the read noise within 30 minutes. No CCD image purge is needed after observations of very bright objects. The Loral devices bleed almost exclusively along the columns.
- **Quantization:** The systematic Analog-to-Digital converter errors have been largely eliminated, contributing to a lower effective read noise.
- **QEH:** Quantum Efficiency Hysteresis (QEH) is not a significant problem in the Loral CCDs because they are frontside illuminated and use MPP operation. The absence of any significant QEH means that the devices do not need to be UV-flooded and the chips can be warmed monthly for decontamination purposes without needing to maintain a UV-flood.
- **Detector MTF:** The Loral devices do suffer from low level detector MTF perhaps caused by scattering in the frontside electrode structure. The effect is to blur images and decrease the limiting magnitude by about 0.5 magnitudes.

1.1.5 UV Imaging

WFPC2 had a design goal of 1% photometric stability at 1470Å over a month. This requires a contamination collection rate of less than 47 ng cm^{-2} $month^{-1}$ on the cold CCD window. Hence, the following features were designed into WFPC2 in an effort to reduce contaminants:

1. Venting and baffling, particularly of the electronics, were redesigned to isolate the optical cavity.
2. There was an extensive component selection and bake-out program, and specialized cleaning procedures.
3. Molecular absorbers (Zeolite) were incorporated.

The CCDs were initially operated at -77˚C after launch, which was a compromise between being as warm as possible for contamination reasons, while being sufficiently cold for an adequate dark rate. However, at this temperature significant photometric errors were introduced by low-level traps in the CCDs. This problem with the charge transfer efficiency of the CCDs has been reduced since 23 April 1994 by operating the CCDs at -88˚C, but this leads to significantly higher contamination rates than hoped for. On-orbit measurements indicate that there is now a decrease in throughput at a repeatable rate of ~30% per month at 1700Å, and moreover, that monthly decontamination procedures are able to remove the contaminants completely and recover this loss.

1.1.6 Aberration Correction and Optical Alignment

WFPC2 contains internal corrections for the spherical aberration of the HST primary mirror. These corrections are made by highly aspheric surfaces figured onto the Cassegrain relay secondary mirror inside each of the four cameras. Complete correction of the aberration depends on a precise alignment between the OTA pupil and these relay mirrors.

Mechanisms inside WFPC2 allow optical alignment on-orbit. The 47˚ pick-off mirror has two-axis tilt capabilities provided by stepper motors and flexure linkages, to compensate for uncertainties in our knowledge of HST's latch positions (i.e., instrument tilt with respect to the HST optical axis). These latch uncertainties would be insignificant in an unaberrated telescope, but must be compensated for in a corrective optical system. In addition, three of the four fold mirrors, internal to the WFPC2 optical bench, have limited two-axis tilt motions provided by electrostrictive ceramic actuators and invar flexure mountings. Fold mirrors for the PC1, WF3, and WF4 cameras are articulated, while the WF2 fold mirror has a fixed invar mounting. A combination of the pick-off mirror and actuated fold mirror (AFMs) has allowed us to correct for pupil image misalignments in all four cameras. Since the initial alignment, stability has been such that mirror adjustments have not been necessary. The mechanisms are not available for GO commanding.

1.2 Which Instrument to Use: WFPC2, FOC, NICMOS, or STIS?

In this section we compare briefly the performance of HST instruments with imaging capability in the UV to near-IR spectral range. As of this writing, both WFPC2 and FOC have capabilities in this area. Two new instruments, the Near-Infrared Camera and Multi-Object Spectrograph (NICMOS) and the Space Telescope Imaging Spectrograph (STIS) should be installed in HST during the second service mission in Early 1997. Important *imaging* parameters for all instruments are summarized in Table 1.1 below.

Table 1.1: Comparison of WFPC2, FOC, NICMOS, and STIS Instrumental Imaging Parameters.

Parameter	WFPC2	FOC[a]	NICMOS	STIS
Wavelength range	1150Å - 11,000Å	1150Å - 6500Å	8000Å - 25,000Å	FUV-MAMA: 1150Å - 1700Å NUV-MAMA: 1700Å - 3100Å CCD: 2000Å - 11,000Å
Detector	Si CCDs	Image Intensifier + EBS TV tube	HgCdTe CCDs	CCD, MAMAs
Image Format	4 x 800 x 800	128 x 128 up to 1024 x 512[b]	3 x 256 x 256	1024 x 1024
Field-of-view and pixel size	150″ x 150″ @ 0.1″ pix^{-1} 34″ x 34″ @ 0.046″ pix^{-1} [c]	up to 7″ x 7″ @ 0.014″ pix^{-1}	1: 11″ x 11″ @ 0.043″ pix^{-1} 2: 19″ x 19″ @ 0.075″ pix^{-1} 3: 51″ x 51″ @ 0.2″ pix^{-1}	MAMAs: 25″ x 25″ @ 0.024″ pix^{-1} CCD: 28″ x 50″ @ 0.05″ pix^{-1} [d]
Read noise	5 e^-	0	30 e^-	MAMAs: 0 e^- CCD: 4e^-
Dark current	0.004 $e^- s^{-1}$	0.0007 $e^- s^{-1}$	<0.1 $e^- s^{-1}$	MAMAs: <0.0001 $e^- s^{-1}$ CCD: 0.004 $e^- s^{-1}$
Saturation	53,000 e^-	2 count $s^{-1}pix^{-1}$	200,000 e^-	MAMAs: 100 count $s^{-1}pix^{-1}$ CCD: 170,000 e^-

a. Parameters given for only F/96 mode. F/48 mode is similar but pixels are twice as large.
b. 1024 x 512 mode uses 0.014″ x 0.028″ pixels to cover 14″ x 14″.
c. "L"-shaped field-of-view using 3 CCDs with 0.1″ pixels, and one CCD with 0.046″ pixels.
d. Field-of-view is 50″ x 50″ if no filter is used, and 12″ x 12″ for some neutral density filters.

1.2.1 Comparison of WFPC2 and FOC

Advantages of each instrument may be summarized as follows.

WFPC2 advantages are:

- Wider field-of-view, 150″ x 150″ vs. 7″ x 7″ or less.
- Higher throughput at λ>4500Å.

- Better flat field accuracy: WFPC2 accuracy of ~1% vs. few % for FOC. WFPC2 has no bright target safety issues, and can give useful data on faint targets near very bright objects. FOC can be damaged by bright objects.
- Better short-term geometric stability: FOC is impacted by geometric changes during turn-on and as a function of orbit position.

FOC advantages are:

- Higher throughput at λ<4500Å.
- Less impacted by far-UV contaminants.
- PSF sampling: FOC offers 0.014″ pixels vs. 0.0455″ on WFPC2.

The choice of instrument will be largely based on wavelength, required field-of-view, and need for good PSF sampling at short wavelengths. We note also that the FOC polarization data should be easier to calibrate, since there are fewer large-angle reflections than WFPC2, and since all polarization angles are available at all positions in the field-of-view.

Table 1.2: Comparison of WFPC2 and FOC Detective Efficiencies.

Instrument	Filter	Mean Wave-length (Å)	Bandpass FWHM (Å)[a]	Peak QE[b]
WFPC2	F122M	1420	100	0.12%
FOC	F140W	1370	298	0.25%
WFPC2	F255W	2586	393	0.45%
FOC	F220W	2280	480	1.2%
WFPC2	F336W	3342	500	2.9%
FOC	F342W	3410	702	5.4%
WFPC2	F439W	4300	700	3.4%
FOC	F430W	3940	832	4.7%
WFPC2	F547M	5476	660	10.6%
FOC	F550M	5460	188	0.83%

a. Note that definition of FWHM is different from “effective width” elsewhere herein.
b. Includes instrument and OTA.

1.2.2 Comparison of WFPC2 and NICMOS

Both WFPC2 and NICMOS are capable of imaging at wavelengths between ~8000Å and ~11,000Å. At longer wavelengths NICMOS must be used; at shorter wavelengths either WFPC2, FOC, or STIS must be used. Table 1.3 below compares the detective efficiency of WFPC2 and NICMOS in the wavelength region where both instruments are viable. Count rates for a V=20 star of spectral class A0 are given for all filters at common wavelengths; the signal-to-noise (S/N) is also given for a 1 hour exposure of this same star. For bright continuum sources WFPC2 and NICMOS offer similar efficiency over the spectral range from 8800Å to 10,500Å; the choice of instrument will likely depend on other factors such as field size and details of the passband shape. However, for very faint sources, the lower read noise of WFPC2 ($5e^-$ for WFPC2 vs. $30e^-$ for NICMOS) should prove advantageous.

Both instruments have a polarimetry capability, but the WFPC2 polarizers are not viable above 8000Å; above this wavelength NICMOS must be used for polarimetry.

Table 1.3: Comparison of WFPC2 and NICMOS Count Rates for V=20 A0 Star.

Instrument	Filter	Mean Wavelength (Å)	Effective Width (Å)	Count Rate (e^{-} s^{-1})	SNR in 1 hour[a]
WFPC2	F785LP	9366	2095	14	215
	F791W	8006	1304	30	314
	F814W	8269	1758	33	333
	F850LP	9703	1670	7.1	150
	FQCH4N (Quad D)	8929	64	0.47	34, 29[b]
	F953N	9546	52	0.21	19, 15[b]
	F1042M	10,443	611	0.20	18, 15[b]
	LRF[c]	8000 9000 9762	105 113 126	1.5 0.64 0.23	66 40 20
NICMOS	F090M[d]	8970	1885	2.0	90
	F095N[d]	9536	88	0.14	12
	F097N[d]	9715	94	0.18	16
	F108N[d]	10,816	94	0.17	15
	F110W (Camera 1)	11,022	5920	6.6	160
	F110W (Camera 2)	11,035	5915	14	260
	F110W (Camera 3)	11,035	5915	26	350

a. WFPC2 SNR assuming two 1800s exposures for cosmic ray removal. NICMOS SNR for central pixel of PSF.
b. Values given for WFC (0.10″ pixels) and PC (0.046″ pixels).
c. LRF filter is continuously tunable from 3710Å to 9762Å. LRF field-of-view is 10″x10″.
d. These NICMOS filters are available only on Camera 1 which has 11″ x 11″ field-of-view.

1.2.3 Comparison of WFPC2 and STIS

Both WFPC2 and STIS are capable of imaging over the same wavelength ranges between ~1150Å and ~11000Å. At much longer wavelengths NICMOS must be used.

Advantages of each instrument may be summarized as follows.

WFPC2 advantages are:

- Wider field-of-view, 150″ x 150″ vs. 50″ x 50″ or less.
- Greater selection of filters, including polarizers.
- Flat field accuracy: WFPC2 is likely to have better flat fielding, since geometry is highly stable. STIS filters are near focal plane and geometry may be unstable due to Mode Selection Mechanism non-repeatability.
- Field uniformity: STIS focus varies across field in image modes.
- Bright Targets: WFPC2 has no bright target safety issues, and can give useful data on faint targets near very bright objects. STIS MAMAs can be damaged by bright objects.

STIS advantages are:

- Much higher UV throughput.
- True solar blind imaging in UV due to MAMA detectors. WFPC2 CCDs are very sensitive to filter red-leak.
- PSF sampling: STIS offers 0.024″ pixels vs. 0.0455″ on WFPC2.
- High time resolution is possible (τ ~125µs) with the MAMA detectors. Also the STIS CCD may be cycled on ~10s timescale using a sub-array.

In general, WFPC2 has a much greater selection of filters and wider field-of-view than STIS, but STIS will have greater detective efficiency in the UV and for its long-pass and unfiltered modes. Table 1.2 below compares the detective efficiency for WFPC2 and STIS filters with similar bandpasses. For UV imaging STIS will be greatly superior due to higher throughput and insensitivity to filter red-leak; only if some detail of a WFPC2 filter bandpass were needed, would it be a viable choice.

For both [OII] 3727Å and [OIII] 5007Å imaging STIS has much higher QE and will be preferred, unless the larger WFPC2 field-of-view is an important factor. The WFPC2 [OIII] filter is wider than its STIS counter-part, which may also be useful for redshifted lines. For broad-band imaging the unfiltered and 5500Å long-pass modes of STIS again will have higher efficiency than WFPC2, though with reduced field-of-view.

Table 1.4: Comparison of WFPC2 and STIS Detective Efficiencies.

Instrument	Filter	Mean Wave-length (Å)	Bandpass FWHM (Å)[a]	Peak QE[b]
WFPC2	F122M	1420	100	0.12%
STIS	F25LYA	1216	85	4.0%
WFPC2	F160BW	1492	500	0.065%
STIS	FUV-MAMA	~1300	300	4.5%
WFPC2	F255W	2586	393	0.45%
STIS	NUV-MAMA	~2400	1300	3.4%
WFPC2	F375N	3738	42	0.8%
STIS	F28X50OII	3740	80	5%
WFPC2	F502N	5013	37	5%
STIS	F28X50OIII	5007	5	15%
WFPC2	F606W	5935	2200	13%
STIS	F28X50LP	~7300[c]	2600	21%
STIS	F50CCD	~5800	4500	22%

a. Note that definition of FWHM is different from “effective width” elsewhere herein.
b. Includes instrument and OTA.
c. 5500Å long pass filter.

1.3 History of WFPC2

The original Wide Field and Planetary Camera (WF/PC-1) served as the prototype for WFPC2. In many respects the two instruments are very similar. Both were designed to operate from 1150Å to 11000Å, both use 800x800 CCD detectors, and both provide spatial samplings of ~0.045″ and ~0.1″ per pixel. The development and construction of WF/PC-1 was led by Prof. J. A. Westphal, Principal Investigator (PI) of the California Institute of Technology. The instrument was built at the Jet Propulsion Laboratory (JPL) and was launched aboard HST in April 1990. It obtained scientific data until it was replaced by WFPC2 during the first service mission in December 1993.

Because of its important role in the overall HST mission, NASA decided to build a second Wide Field and Planetary Camera (WFPC2) as a backup clone of

WF/PC-1 even before HST was launched. WFPC2 was already in the early stages of construction at JPL when HST was launched. After the discovery of spherical aberration in the HST primary mirror, it was quickly realized that a modification of the WFPC2 internal optics could correct the aberration and restore most of the originally expected imaging performance. As a result, development of WFPC2 was accelerated. Dr. J. T. Trauger of JPL is the project PI for WFPC2 and led the Investigation Definition Team (IDT).

The WFPC2 completed system level thermal vacuum (SLTV) testing at JPL in April and May 1993. Between June and November there were payload compatibility checks at Goddard Space Flight Center (GSFC), and payload integration at Kennedy Space Center (KSC). WF/PC-1 was replaced by WFPC2 during the first Servicing Mission in December 1993. WFPC2 was shown to meet most of its engineering and scientific performance requirements by testing conducted during the three month Servicing Mission Observatory Verification (SMOV) period following the servicing mission. The General Observer community has had access to WFPC2 since the start of Cycle 4 in January 1994.

WFPC2 accurately corrects the HST spherical aberration, is a scientifically capable camera configured for reliable operation in space without maintenance, and is an instrument which can be calibrated and maintained without excessive operational overhead. It incorporates evolutionary improvements in photometric imaging capabilities. The CCD sensors, signal chain electronics, filter set, UV performance, internal calibrations, and operational efficiency have all been improved through new technologies and lessons learned from WF/PC-1 operations and the HST experience since launch.

WFPC2 SMOV requirements were developed by the IDT, GSFC, and the STScI to include: verification of the baseline instrument performance; an optical adjustment by focusing and aligning to minimize coma; the estimation of residual wavefront errors from the analysis of star images; a photometric calibration with a core set of filters (including both visible and UV wavelengths); and the evaluation of photometric accuracy and stability over the full field with the core filter set. The results of these studies are documented in Holtzman, et al., 1995a and 1995b, and are summarized in this Handbook.

Despite these successes, the first years of scientific operation of WFPC2 have revealed a number of relatively minor instrumental defects that were not expected from the pre-launch testing. These include a low-level charge transfer inefficiency, a higher than expected level of scattered light around bright objects, and variable and lower than expected ultraviolet (UV) efficiency. In addition, we have come to understand the instrument more fully -- particularly in terms of its overall photometric performance, geometric distortion, scale and alignments, hot pixels, and CCD traps. All of this new information is described here.

1.4 The Previous vs. Current Generation: WF/PC-1 vs. WFPC2

For historical reasons, it is useful to offer comparisons between the current WFPC2, and its predecessor WF/PC-1, which was returned to Earth in December 1993.

- **Field format:** WF/PC-1 contained 8 cameras and CCDs, each CCD having 800 x 800 pixels. Four were used in the Planetary Camera mode (0.043″ pixels), and four were used in the Wide Field Camera mode (0.10″ pixels). The two pixel formats were selected by rotating the pyramid mirror by 45°. WFPC2 budget and schedule constraints forced a reduction from 8 to 4 camera channels in August 1991. WFPC2 contains only 4 CCDs; the pyramid mirror is fixed and the 4 cameras are physically located in the bays occupied by the WF/PC-1 WFC.
- **Aberration correction:** WF/PC-1 contained no correction for spherical aberration of the OTA primary mirror. Only about 15% of light from a stellar target fell into the core of the PSF (diameter ~0.1″). WFPC2 incorporates corrective figures on the Cassegrain secondary mirrors inside the relay cameras, and as a result places ~60% of the light from a star inside a diameter of 0.1″. Precise alignment of the OTA pupil on these mirrors is required to attain full correction of the spherical aberration. Hence the pick-off mirror (POM) is steerable in WFPC2, and three of the fold mirrors contain tip-tilt actuators.
- **CCD Technology:** Many properties of WF/PC-1 and WFPC2 CCDs are compared in Table 4.1 on page 65. Many differences derive from the fact that the WF/PC-1 CCDs were thinned, backside illuminated devices whereas the WFPC2 CCDs are thick, frontside illuminated devices. WF/PC-1 CCDs were thinned and backside illuminated. The active silicon layer was a free-standing membrane somewhat less than 10µm thick, with photons impinging directly on the silicon layer, without attenuation in the polysilicon gate structure built on the other ('front') side of the device.
- **Quantum Efficiency Hysteresis (QEH):** The WF/PC-1 CCD's required a UV flood procedure and continuous cold temperatures to avoid QEH and hence non-linearity. A UV flood was performed early in the WF/PC-1 mission, but could not be repeated due to problems with the HST magnetometers. This in turn limited the temperature range allowable during decontaminations, since high temperatures would remove the UV flood, which in turn severely limited UV science capabilities. Some QE instability was also seen, particularly in the B band, due to changes in the UV flood. WFPC2 CCDs support multi-pinned phase (MPP) operation which eliminates quantum efficiency hysteresis.
- **Charge Transfer Efficiency:** WF/PC-1 devices suffered from significant charge transfer efficiency (CTE) errors at image intensities below ~200 electrons per pixel. This was overcome by preflashing virtually all science images. WFPC2 devices have very little CTE error, and hence no preflash is

used. Low-level charge traps are present in the WFPC2 devices, and result in a loss of about 4% of the signal when a star image is clocked down through all rows of the CCD. In the presence of background, the effect is reduced. For most applications, CTE is negligible or calibratable and pre-flash exposures are not required.

- **Detector MTF:** The WFPC2 Loral devices do suffer from poorer CCD detector MTF than the WF/PC-1 CCDs, perhaps caused by scattering in the frontside electrode structure. The effect is to blur images and decrease the limiting magnitude by about 0.5 magnitudes.
- **Flat field quality:** WF/PC-1 CCDs were chemically thinned devices and therefore varied in thickness across the field-of-view causing large features in the flat fields. WFPC2 CCDs are un-thinned and the intrinsic response is uniform to ~3% across the field.
- **DQE:** The WFPC2 CCDs have intrinsically lower QE than WF/PC-1 CCDs above 4800Å, which is due to attenuation by frontside electrode structures.
- **Gain switch:** WF/PC-1 had only a single analog-to-digital converter gain setting of 8 $e^- DN^{-1}$ which saturated at about 30,000e^-. Two gains are available with WFPC2: a 7 $e^- DN^{-1}$ channel which gives reasonable sampling of the 5e^- read noise, and which saturates at about 27,000e^-, and a 14 $e^- DN^{-1}$ channel which saturates at about 53,000e^- and extends the useful dynamic range.
- **Quantization:** The systematic analog-to-digital converter errors that were present in the low order bits on WF/PC-1 have been largely eliminated, contributing to a lower effective read noise in WFPC2.
- **Calibration Channel:** WF/PC-1 contained a solar UV flood channel which was physically in the location of the present WFPC2 calibration channel. This transmitted solar UV light into the camera to provide a UV flood capability.
- **Entry Port:** The WF/PC-1 camera was sealed by an afocal MgF_2 window immediately behind the shutter. The WFPC2 entry port is open.
- **Chronographic Capability:** WF/PC-1 contained a low reflectance spot on the pyramid (known as the Baum spot) which could be used to occult bright objects. This has been eliminated from WFPC2, since the spherical aberration severely reduces its utility.
- **Contamination Control:** Since launch, WF/PC-1 suffered from the accumulation of molecular contaminants on the cold (-87˚C) CCD windows. This molecular accumulation resulted in the loss of FUV (1150-2000Å) throughput and attenuation at wavelengths as long as 5000Å. Another feature of the contamination was the “measles” — multiple isolated patches of low volatility contamination on the CCD window. Measles were present even after decontamination cycles, when most of the accumulated molecular contaminants were boiled off by warming the CCDs. In addition to preventing UV imaging, these molecular contamination layers scattered light and seriously impacted the calibration of the instrument. WFPC2 has far

less contamination than WF/PC-1 owing to pre-launch cleaning and bake-out procedures, careful design of venting paths to protect the optical bench area, and inclusion of Zeolite molecular absorbers in the design. There is now a decrease in throughput of about 30% per month at 1700Å, but monthly decontamination procedures completely remove this material. This throughput drop is also highly predictable and can be calibrated out during photometric analyses.

1.5 Organization of this Handbook

A description of the instrument is contained in Chapter 2. The filter set is described in Chapter 3. CCD performance is discussed in Chapter 4. A description of the Point Spread Function is given in Chapter 5. The details necessary to estimate exposure times are described in Chapter 6. A summary of observation strategies is given in Chapter 7. Data products and standard calibration methods, and calibration plans are summarized in Chapter 8. A complete list of references is given in Chapter 9.

This document summarizes the performance of the WFPC2 as known in April 1996 after two years of on-orbit calibration. Observers are encouraged to contact the STScI Help Desk, the WFPC2 WWW pages (see section 1.7 “WFPC2 Handbook on the WWW” below), and STScI Instrument Scientists for the latest information.

1.6 What’s New in Version 4.0

Major revisions since Version 3.0 may be summarized as follows:

- Comparisons to FOC, STIS, and NICMOS.
- Observation Strategies: A new chapter (Ch. 7) has been added specifically to assist observers in preparing Phase II proposals.
- Exposure Time Estimation: Ch. 6 has been largely re-written. Signal-to-noise ratio equations for Poisson-limited, background-limited, and generalized cases are now included for point sources (both with PSF fitting and aperture photometry) and extended sources. The WWW on-line Exposure Time Calculator program is briefly described. A new Appendix gives representative SNR values for various exposures of stellar, power law, and emission line sources.
- CCD Performance: Material on dark current and CTE (charge transfer efficiency) has been updated.
- Calibration: Material on UV throughput, dark current calibration, flat fielding, and impact of focus variations on photometry has been updated. Cycle 6 calibration proposals are described.

- Other changes include addition of an index and an acronym list.

1.7 WFPC2 Handbook on the WWW

This Handbook will appear on the WFPC2 WWW pages accessible at:

`http://www.stsci.edu/ftp/instrument_news/WFPC2/top_wfpc2.html`

and will be updated as new information becomes available.

1.8 The Help Desk at STScI

STScI maintains a Help Desk whose staff quickly provide answers to any HST-related topic, including questions about WFPC2 and the Cycle 7 proposal process. The Help Desk staff has access to all of the resources available at the Institute. They maintain a database of frequently asked questions and answers, so that many questions can be answered immediately. The Help Desk staff can also provide copies of STScI documentation, in either hardcopy or electronic form, including Instrument Science Reports and Instrument Handbooks.

Questions sent to the Help Desk during normal business hours are usually answered within one hour. Questions received outside normal business hours will be answered within the first two hours of the next business day. Usually, the Help Desk staff will reply with the answer to a question, but occasionally they will need more time to investigate the answer. In these cases, they will reply with an estimate of the time needed to reply with the full answer.

We ask that you please send *all* initial inquiries to the Help Desk. If your question requires a WFPC2 Instrument Scientist to answer it, the Help Desk staff will put a WFPC2 Instrument Scientist in contact with you. By sending your request to the Help Desk, you are guaranteed that someone will provide a timely response.

To contact the Help Desk at STScI:

- **Send e-mail:** `help@stsci.edu`
- **Phone:** 1-410-338-1082

The Space Telescope European Coordinating Facility (ST-ECF) also maintains a Help Desk. European users should generally contact the ST-ECF for help; all other users should contact STScI.

To contact the ST-ECF Help Desk in Europe:

- **Send e-mail:** `stdesk@eso.org`.

1.9 Further Information

The material contained in this Handbook is derived from ground tests and design information obtained by the IDT and the engineering team at JPL, and from on-orbit measurements. Other sources of information are listed below. A complete list of references appears on page 197.

- *HST Phase II Proposal Instructions*, (Version 8.0, 15 December 1995).[1]
- *HST Data Handbook*, (Version 2.0, December 1996).[1]
- *Calibrating Hubble Space Telescope: Post Service Mission* (1995).[1]
- *STSDAS Calibration Guide*, (November 1991).[1]
- *The Reduction of WF/PC Camera Images*, Lauer, T., P.A.S.P. 101, 445 (1989).
- *The Imaging Performance of the Hubble Space Telescope*, Burrows, C. J., et. al., Ap. J. Lett., 369, L21 (1991).
- Interface Control Document (ICD) 19, “PODPS to STSDAS”
- Interface Control Document (ICD) 47, “PODPS to CDBS”
- *The Wide Field/Planetary Camera in The Space Telescope Observatory*, J. Westphal and the WF/PC-1 IDT, IAU 18th General Assembly, Patras, NASA CP-2244 (1982).
- *The WFPC2 Science Calibration Report*, Pre-launch Version 1.2, J. Trauger, editor, (1993). [IDT calibration report]
- *White Paper for WFPC2 Far-Ultraviolet Science*, J. T. Clarke and the WFPC2 IDT (1992)[1].
- *The Performance and Calibration of WFPC2 on the Hubble Space Telescope*, Holtzman, J., et al., P.A.S.P., 107, 156 (1995).
- *The Photometric Performance and Calibration of WFPC2*, Holtzman, J., et al., P.A.S.P., 107, 1065 (1995).
- The Institute’s WFPC2 World Wide Web page at address: `http://www.stsci.edu/ftp/instrument_news/WFPC2/wfpc2_top.html`
- The Institute’s WFPC2 Space Telescope Analysis Newsletter (STAN), which is distributed monthly via e-mail, and provides notification of any changes in the instrument or its calibration. To subscribe, send e-mail to `help@stsci.edu`.

1. These documents may be requested by e-mail from `help@stsci.edu`.

CHAPTER 2: Instrument Description

In This Chapter...

Science Objectives / 19
WFPC2 Configuration, Field-of-View, and Resolution / 20
Overall Instrument Description / 21
Quantum Efficiency / 24
Shutter / 26
Serial Clocks / 27
Overhead Times / 29
CCD Orientation and Readout / 31
Calibration Channel / 33

2.1 Science Objectives

The scientific objective of the WFPC2 is to provide photometrically and geometrically accurate images of astronomical objects over a relatively wide field-of-view (FOV), with high angular resolution across a broad range of wavelengths.

WFPC2 meets or exceeds the photometric performance of WF/PC-1 in most areas. The goal is 1% rms photometric accuracy, which means that the relative response in all 800x800 pixels per CCD must be known to better than 1% through each filter, and that standard calibrations be done at this level. Currently, the absolute calibration in the primary broadband photometric filters is accurate at around the 2% level, and is expected to continue to improve. Success in this area is dependent on the stability of all elements in the optical train, particularly the CCDs and filters.

The narrow point spread function is essential to all science programs being conducted with the WFPC2, because it allows one to both go deeper than ground based imagery, and to resolve smaller scale structure with higher reliability and dynamic range. Further, many of the scientific goals which originally justified the HST require that these high quality images be obtained across a wide field-of-view. The Cepheid distance scale program, for example, cannot be accomplished without a relatively wide field-of-view.

A unique capability of the WFPC2 is that it provides a sustained, high resolution, wide field imaging capability in the vacuum ultraviolet. Considerable effort has been expended to assure that this capability is maintained. Broad passband far-UV filters, including a Sodium Wood's filter, are included. The Wood's filter has superb red blocking characteristics. Photometry at wavelengths short of 3000Å is improved through the control of internal molecular contamination sources and the ability to put the CCDs through warm-up decontamination cycles without loss of prior calibrations.

While the WFPC2 CCDs have lower V-band quantum efficiency than the WF/PC-1 chips, for many applications this is more than made up for by the lower read noise, and by the intrinsically uniform flat field. For example, these characteristics are expected to increase the accuracy of stellar photometry, which was compromised by uncertainty in the flat field in WF/PC-1.

2.2 WFPC2 Configuration, Field-of-View, and Resolution

The field-of-view and angular resolution of the wide field and planetary camera is split up as follows (see Section 4.2 for more details on CCDs):

Table 2.1: Summary of Camera Format.

Camera	Pixel and CCD Format	Field-of-View	Pixel Scale	F/ratio
Wide Field	$800 \times 800 \times 3$ CCDs	$2.5' \times 2.5'$ (L-shaped)	~100 milli-arcseconds	12.9
Planetary	$800 \times 800 \times 1$ CCD	$35'' \times 35''$	~46 milli-arcseconds	28.3

Figure 2.1: Wide Field Planetary Camera Concept Illustration. The calibration channel, and pick-off mirror mechanisms are not shown.

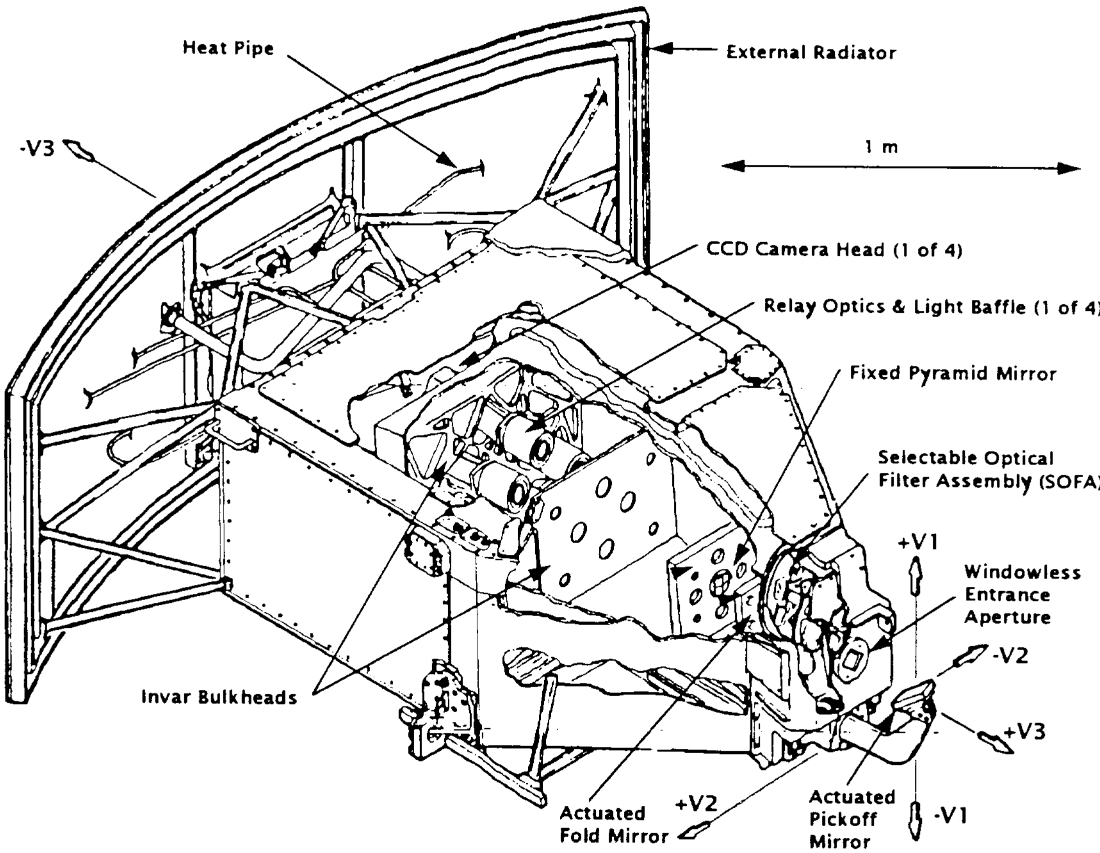

2.3 Overall Instrument Description

The Wide-Field and Planetary Camera, illustrated in Figure 2.1, occupies the only radial bay allocated to a scientific instrument. Its field-of-view is centered on the optical axis of the telescope and it therefore receives the highest quality images. The three Wide-Field Cameras (WFC) at F/12.9 provide an “L” shaped field-of-view of 2.5x2.5 arcminutes with each 15 μm detector pixel subtending 0.10″ on the sky. In the Planetary Camera (PC) at F/28.3, the field-of-view is 35″ x 35″, and each pixel subtends 0.046″. The three WFCs undersample the point spread function of the Optical Telescope Assembly (OTA) by a factor of 4 at 5800Å in order to provide an adequate field-of-view for studying galaxies, clusters of galaxies, etc. The PC resolution is over two times higher. Its field-of-view is adequate to provide full-disk images of all the planets except Jupiter (which is 47″ in maximum diameter). The PC has numerous extra-solar applications, including studies of galactic and extra-galactic objects in which both high angular resolution and excellent sensitivity are needed. In addition to functioning as the prime instrument, the WFPC2 can be used for target acquisition in support of other HST instruments, or for parallel observations.

Figure 2.2 shows the optical arrangement (not to scale) of the WFPC2. The central portion of the OTA F/24 beam is intercepted by a steerable pick-off mirror attached to the WFPC2, and is diverted through an open entry port into the instrument. The beam then passes through a shutter and filters. A total of 48 spectral elements and polarizers are contained in an assembly of 12 filter wheels. Then the light falls onto a shallow-angle, four-faceted pyramid located at the aberrated OTA focus, each face of the pyramid being a concave spherical surface. The pyramid divides the OTA image of the sky into four parts. After leaving the pyramid, each quarter of the full field-of-view is relayed by an optical flat to a Cassegrain relay that forms a second field image on a charge-coupled device (CCD) of 800x800 pixels. Each detector is housed in a cell that is sealed by a MgF_2 window. This window is figured to serve as a field flattener.

The aberrated HST wavefront is corrected by introducing an equal but opposite error in each of the four Cassegrain relays. An image of the HST primary mirror is formed on the secondary mirrors in the Cassegrain relays. (The fold mirror in the PC channel has a small curvature to ensure this, and is why the PC magnification changed from F/30 in WF/PC-1 to F/28.3 in WFPC2.) The spherical aberration from the telescope's primary mirror is corrected on these secondary mirrors, which are extremely aspheric. The point spread function is then close to that originally expected for WF/PC-1.

Figure 2.2: WFPC2 Optical Configuration

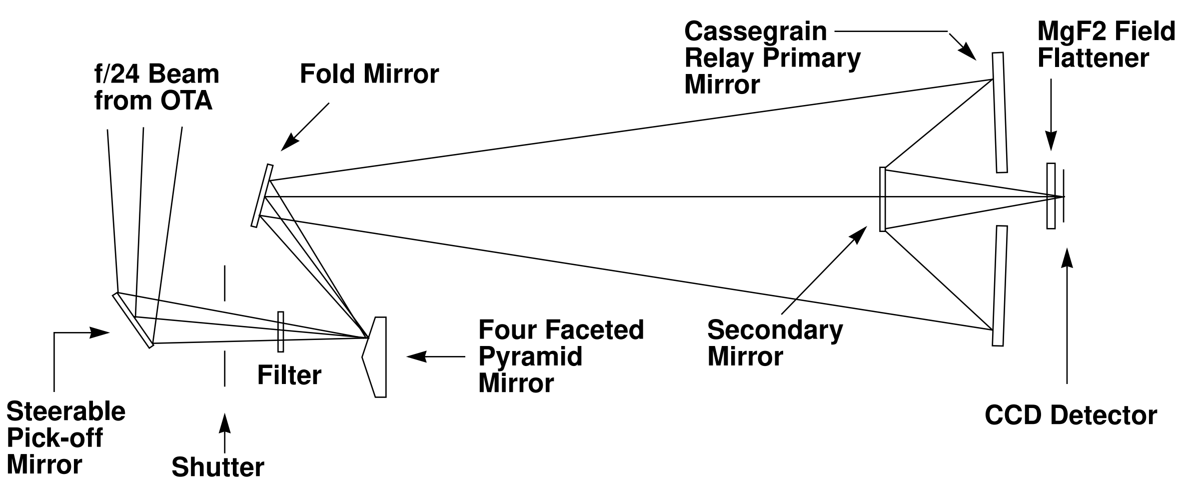

The single most critical and challenging technical aspect of applying a correction is assuring exact alignment of the WFPC2 pupils with the pupil of the HST. If the image of the HST primary does not align exactly with the repeater secondary, the aberrations no longer cancel, leading to a wavefront error and comatic images. An error of only 2% of the pupil diameter produces a wavefront error of 1/6 wave, leading to degraded spatial resolution and a loss of about 1 magnitude in sensitivity to faint point sources. This error corresponds to mechanical tolerances of only a few microns in the tip/tilt motion of the pick-off mirror, the pyramid, and the fold mirrors.

Mechanisms inside WFPC2 allow optical alignment on-orbit; these are necessary to insure correction of the OTA spherical aberration. The beam alignment is set with a combination of the steerable pick-off mirror and actuated fold mirrors in cameras PC1, WF3 and WF4. The 47° pick-off mirror has two-axis tilt capabilities provided by stepper motors and flexure linkages, to compensate for uncertainties in our knowledge of HST's latch positions (i.e., instrument tilt with respect to the HST optical axis). These latch uncertainties would be insignificant in an unaberrated telescope, but must be compensated for in a corrective optical system. In addition, three of the four fold mirrors, internal to the WFPC2 optical bench, have limited two-axis tilt motions provided by electrostrictive ceramic actuators and invar flexure mountings. Fold mirrors for the PC1, WF3, and WF4 cameras are articulated, while the WF2 fold mirror has a fixed invar mounting. A combination of the pick-off mirror and fold mirror actuators has allowed us to correct for pupil image misalignments in all four cameras. Since the initial alignment, stability has been such that mirror adjustments have not been necessary. The mechanisms are not available for GO commanding.

The WFPC2 pyramid cannot be focused or rotated. WFPC2 is focused by moving the OTA secondary mirror, and then COSTAR (or any future science instruments) is adjusted to achieve a common focus for all the HST instruments.

The four CCDs provide a 1600 x 1600 pixel field-format; three of the 800 x 800 CCDs have 0.1″ pixels (WFC), and one has 0.046″ pixels (PC). The CCDs are physically oriented and clocked so that the pixel read-out direction is rotated approximately 90° in succession (see Figure 1.1 on page 2). The (1,1) pixel of each CCD array is thereby located near the apex of the pyramid. As a registration aid in assembling the four frames into a single picture, a light can be turned on at the pyramid to form a series of eleven fixed artificial "stars" (known as Kelsall spots or K-spots) along the boundaries of each of the quadrants. This calibration is normally done in a separate exposure. The K-spot images are aberrated and similar in appearance to the uncorrected HST PSF. The relative alignment of the four channels has been more accurately determined from star fields, and is stable over long periods, but the K-Spot images are useful for verifying the stability.

Figure 2.3: Cooled Sensor Assembly

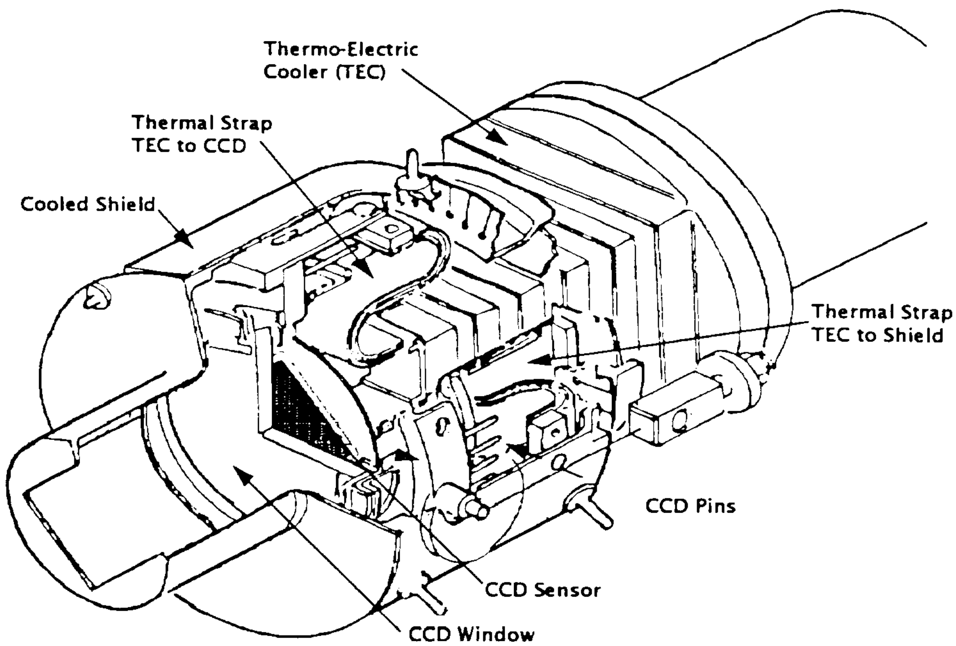

Each CCD is a thick frontside-illuminated silicon sensor, fabricated by Loral Aerospace. A CCD, mounted on its header, is hermetically packaged in a ceramic-tube body that is filled with 1.1 atmosphere of argon to prevent degradation of the UV sensitive phosphor, and sealed with the MgF_2 field flattener. This complete cell is connected with compliant silver straps to the cold junction of a thermo-electric cooler (TEC). The hot junction of the TEC is connected to the radial bay external radiator by an ammonia heat pipe. This sensor-head assembly is shown in Figure 2.3. During operation, each TEC cools its sensor package to suppress dark current in the CCD.

2.4 Quantum Efficiency

The WFPC2 provides useful sensitivity from 1150Å to 11000Å in each detector. The overall spectral response of the system is shown in Figure 2.4 (not including filter transmissions). The curves represent the probability that a photon that enters the 2.4m diameter HST aperture at a field position near the center of one of the detectors will pass all the aperture obscurations, reflect from all the mirrors, and eventually be detected as an electron in the CCD. The throughput of the system combined with each filter is tabulated in Table 6.1 and also shown in the Appendix.

Figure 2.4: WFPC2 + OTA System Throughput. These measurements made on orbit are much more accurate than the pre-launch estimates, and are used consistently throughout this Handbook.

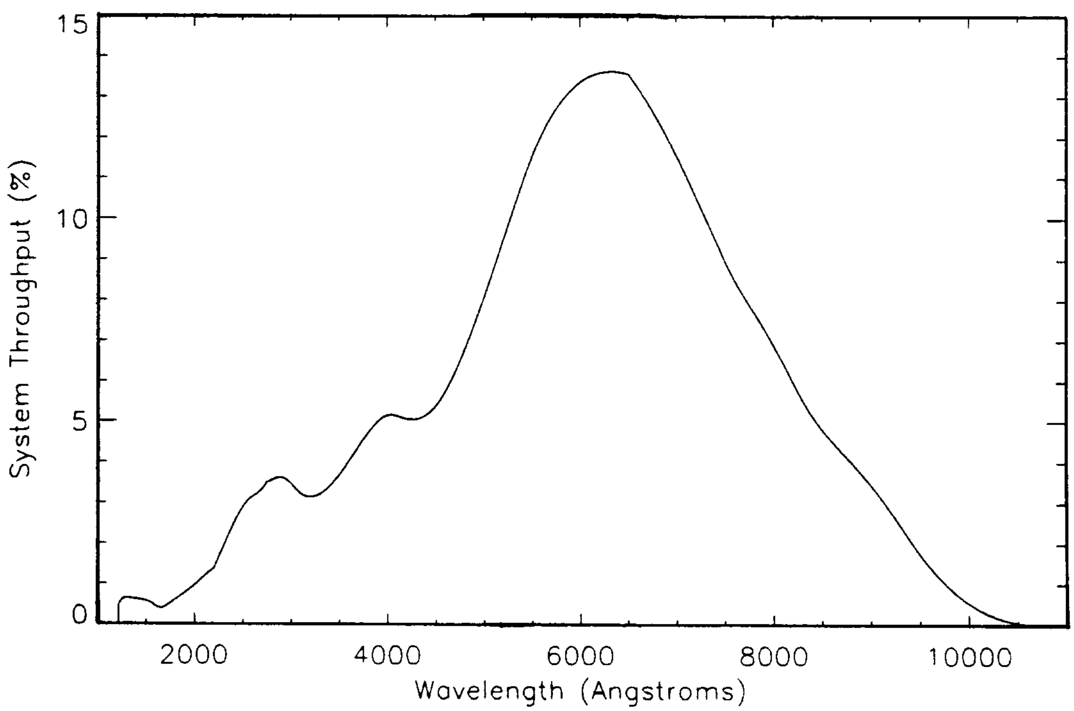

The visible and red sensitivity of the WFPC2 is a property of the silicon from which the CCDs are fabricated. To achieve good ultraviolet response, each CCD is coated with a thin film of Lumogen, a phosphor. Lumogen converts photons with wavelengths less than 4800Å into visible photons with wavelengths between 5100Å and 5800Å, which the CCD detects with good sensitivity. Beyond 4800Å, the Lumogen becomes transparent and acts to some degree as an anti-reflection coating. Thus, the full wavelength response is determined by the MgF_2 field flattener cutoff on the short-wavelength end and the silicon band-gap in the infrared at 1.1 eV (~11000Å).

With the WFPC2 CCD sensors, images may be obtained in any spectral region defined by the chosen filter with high photometric quality, wide dynamic range, and excellent spatial resolution. The bright end of the dynamic range is limited by the 0.11 seconds minimum exposure time, and by the saturation level of the analog-to-digital converter (ADC) at the chosen gain, which is roughly 53000 (gain=14, though called ADT-GAIN=15 in RPS2) or 27000e^- (gain=7) per pixel. The maximum signal-to-noise ratio corresponding to a fully exposed pixel will be about 230. The faint end of the dynamic range is limited by photon noise, instrument read noise and, for the wide-band visible and infra-red filters, the sky background.

Table 2.2 gives characteristic values of the expected dynamic range in visual magnitudes for point sources. The minimum brightness is given for an integrated

S/N ratio of 3, and the maximum corresponds to CCD ADC saturation (selected as 53000e$^-$). The quoted values assume an effective bandwidth of 1000Å at about 5600Å (filter F569W). The planets and many other resolved sources are observable in this filter with short exposures even if their integrated brightness exceeds the 8.5 magnitude limit.

Table 2.2: WFPC2 Dynamic Range in a Single Exposure.

Configuration	Exposure (seconds)	Min. V Magnitude	Max. V Magnitude
Wide Field	0.11	8.82	17.83
Wide Field	3000.	19.91	28.14
Planetary	0.11	8.40	17.47
Planetary	3000.	19.49	28.20

2.5 Shutter

The shutter is a two-blade mechanism used to control the duration of the exposure. A listing of the possible exposure times is contained in Table 2.3. These are the only exposure times which can be commanded. Current policy is to round down non-valid exposure times to the next valid value. An exposure time of less than 0.11 seconds will therefore only result in a bias frame being taken.

Some exposures should be split into two (CR-SPLIT) in order to allow cosmic ray events to be removed in post-processing. By default, exposures of more than 10 minutes are CR-SPLIT. If an exposure is CR-SPLIT, the exposure time is divided into two fractions and then rounded down. Normally the fractional split is 50%/50% but, unless constrained by the user with CR-TOLERANCE, the ratio may be up to 70%/30%, as allowed by the default CR-TOLERANCE=0.2. Note that some exposure times in the table do not correspond to commandable values when halved. In preparing a proposal containing an exposure that is to be CR-SPLIT, the simplest procedure to use in order to be sure of a given total exposure time, is to enter double a legal value, and impose CR-TOLERANCE =0.

For the shortest exposure times, it is possible to reconstruct the actual time of flight of the shutter blades. Encoder disks, attached to the shutter blade arms, are timed by means of a photo-transistor. The maximum error is 5 milliseconds. The necessary information is contained in the WFPC2 engineering data stream, however, this information is not in the processed science header.

Diffraction effects from the edges of the shutter blades affect the point spread function for very short exposures. It is advisable to use exposure times greater than 0.2 second when obtaining point spread functions in support of long exposure observations (see the WF/PC-1 IDT OV/SV Report, Chapter 9, for further discussion in the spherically aberrated case).

The control of the initial opening of the WFPC2 shutter during an observation is held by the internal WFPC2 microprocessor in all cases. However, control over when the shutter is closed is held by the microprocessor only for exposures less than 180 seconds in duration. For longer exposures, control passes to the Application Processor (AP-17) in the NSSC-1 spacecraft computer. The consequence of this arrangement is that loss of guide star lock will result in the WFPC2 shutter being closed only for those observations with planned durations of 180 seconds or longer. The AP-17 always controls the shutter closing if the serial clocks are enabled during the exposure (CLOCKS=YES), which then has a minimum planned duration of 1 second, and exposures are rounded to the nearest second. If guide star lock is reacquired prior to the end of the planned observation time, the shutter will reopen to obtain a portion of the planned integration. As discussed in the next section, CLOCKS=YES should generally not be used with exposures shorter than 30 sec., if 1% or better photometric accuracy is needed.

Table 2.3: Quantized Exposure Times (Seconds). Exposure times where the PSF is affected by shutter flight time are underlined. Exposures normally without loss of lock checking are in italics. Times that are CR-Split by default are in boldface. Exposures that take more than one orbit even when CR-split are not normally accessible to GOs and are crossed (and exposures longer than 5400 seconds must be CR-Split). Exposure times that should not be used when CLOCKS=YES are shaded.

0.11	*0.4*	*2.0*	*10.*	*40.*	200.	**900.**	**1900.**	**2900.**	**3900.**	**4900.**	**6200.**	~~**15000.**~~
0.12	*0.5*	*2.3*	*12.*	*50.*	230.	**1000.**	**2000.**	**3000.**	**4000.**	**5000.**	**6400.**	~~**20000.**~~
0.14	*0.6*	*2.6*	*14.*	*60.*	260.	**1100.**	**2100.**	**3100.**	**4100.**	**5100.**	**6600.**	~~**25000.**~~
0.16	*0.7*	*3.0*	*16.*	*70.*	300.	**1200.**	**2200.**	**3200.**	**4200.**	**5200.**	**6800.**	~~**30000.**~~
0.18	*0.8*	*3.5*	*18.*	*80.*	350.	**1300.**	**2300.**	**3300.**	**4300.**	**5300.**	**7000.**	~~**40000.**~~
0.20	*1.0*	*4.0*	*20.*	*100.*	400.	**1400.**	**2400.**	**3400.**	**4400.**	**5400.**	**7500.**	~~**50000.**~~
0.23	*1.2*	*5.0*	*23.*	*120.*	500.	**1500.**	**2500.**	**3500.**	**4500.**	**5500.**	**8000.**	~~**75000.**~~
0.26	*1.4*	*6.0*	*26.*	*140.*	600.	**1600.**	**2600.**	**3600.**	**4600.**	**5600.**	**8500.**	~~**100000.**~~
0.30	*1.6*	*7.0*	*30.*	*160.*	**700.**	**1700.**	**2700.**	**3700.**	**4700.**	**5800.**	**9000.**	
0.35	*1.8*	*8.0*	*35.*	180.	**800.**	**1800.**	**2800.**	**3800.**	**4800.**	**6000.**	**10000.**	

2.6 Serial Clocks

The serial transfer registers of the CCDs can be kept running during an exposure (CLOCKS=YES), or run only during the readout (CLOCKS=NO, the default).

The serial clocks are sometimes used on very bright targets where extensive blooming of the up and down the CCD columns is expected. CLOCKS=YES causes charge which blooms to the ends of the CCD to be read out and disposed of, thus preventing it from flowing back into the image. They will be useful when any single CCD column contains in excess of ~10^8 electrons. Note that the serial clocks do not actually suppress the blooming process, instead they merely remove any charge that blooms to the top or bottom of the CCD.

For most circumstances, we recommend CLOCKS=NO. The reasons for this recommendation are:

1. CLOCKS=YES is not widely used, so anomalies may exist or develop that we are not aware of. Also, this mode is not as well calibrated as CLOCKS=NO (although we expect the calibration to be independent of the state of the clocks).
2. The shutter open time when CLOCKS=YES can have significant errors. In this mode, there are delays of up to 0.25 seconds in opening the shutter (which are not present when CLOCKS=NO). This means that for exposures of less than ~30 seconds, there may be photometric errors greater that 1%, unless special precautions are taken in the data reduction. Furthermore, if a non-integral exposure time is specified in the proposal, it will be rounded to the nearest second. See below for details.

On the other hand:

1. We do advise CLOCKS=YES if you expect star images to be so saturated that a significant amount of charge will bleed off the chip during the exposure. This would mean that you expect much more than 10^8 electrons from at least one star in the exposure (more than 1000 pixels would be saturated). Otherwise the charge can be detected in other parts of the image.
2. One advantage of CLOCKS=YES is that the overhead time is 1 minute less for exposures longer than 180 seconds. This can be significant if you have a large number of exposure times in the 3 to 10 minute range.
3. Unlike the original WF/PC-1, we do not see a significant variation of WFPC2 dark level with CLOCKS=YES.

In summary:

0-0.8 sec	CLOCKS=NO is required.
1 - 30 sec	Use CLOCKS=NO (or attempt photometric corrections during the analysis of the data).
20 - 180 sec	Use CLOCKS=NO unless more than 10^8 detected electrons from a single star are expected.
180+ sec	Use CLOCKS=NO unless more than 10^8 detected electrons are expected, or if you need to save 1 minute of overhead.

While exposure times are corrupted for CLOCKS=YES, and are not accurately reported in the image headers, correct values can be computed. Details are as follows:

1. Non-integer exposure times <3 minutes are rounded to the nearest integer (e.g., 1.2 sec and 1.4 sec will actually be 1.0 sec long, 3.5 sec exposures take 4.0 sec). This roundoff is due to the way the spacecraft computer monitors the take-data flag (AP-17 uses its own integer-based timecode). This rounding is reflected properly in the header keywords (keywords UEXPODUR, EXPSTART, EXPEND, EXPTIME, and EXPFLAG in the `.c0h` file headers, or UEXPODUR and CMD_EXP in the `.shh` headers).
2. All CLOCKS=YES exposures are also shortened by either 0.125 or 0.250 seconds. This decrease in exposure time is ***not*** reflected in the file headers; the amount depends upon which shutter blade was in place at the start of the exposure. The decrease in exposure time is due to the manner in which the application processor (AP-17) in the spacecraft computer operates the shutter blades. When CLOCKS=NO (default), the WFPC2 microprocessor opens the shutter, the AP-17 closes the shutter, and the exposure time is as requested. However, with CLOCKS=YES, the AP-17 opens the shutter, first blade A, then blade B. If blade A is closed at the start of the exposure, the actual exposure begins 0.125 seconds after the AP-17 issues the blade command. If blade B is closed at the exposure start, the exposure starts 0.250 seconds later (after the AP-17 sends the open-A command followed by open-B). The shutter in place at exposure start is given in the SHUTTER keyword in the `.c0h` file.

2.7 Overhead Times

Efficient use of the WFPC2 requires an understanding of the overhead times of the instrument. In this section, the various causes of overhead are presented in a manner that should allow the user to make a fairly accurate prediction of the cost in time of a given sequence of exposures. This information is provided for completeness and background. Guidelines in the Phase I proposal instructions and RPS2 should be followed to develop Phase I and II proposals, respectively. (See also “Choosing Exposure Times” on page 152.)

1. Telescope alignments. A telescope alignment is, in practice, a set of images uninterrupted by a POS_TARG target position change or the end of orbit. The start of an alignment requires 1 minute overhead in order to synchronize timing with a major frame (all commands to the instrument take place on major frames which last 1 minute). The end of alignment uses one minute for tape recorder overhead. If scans are being performed, another minute of overhead is required and, if images are requested in real-time, another 2 minutes must be added to the alignment end. There are additional overheads at the start of each target visibility period associated with guide star acquisition (9 minutes), or reacquisition (6 minutes).
2. Filter changes. A filter change requires at least 1 minute, the use of 2 filters requires 2 minutes of overhead. Furthermore, since the filter history is lost across telescope alignments, at least one minute is spent on selecting the fil-

ter at an alignment start, regardless of the filter in place before the alignment.

3. CCD clearing. Clearing the CCD is done before every exposure and requires 14 seconds. This time is part of the first major frame of the exposure. Therefore, time taken for a given exposure (excluding all other overheads) is the exposure time plus 14 seconds rounded up to the next integral minute. For example, all legal exposure times up to 40 seconds inclusive cost one minute.

4. CCD readout. The readout time for an exposure is one minute. An additional minute is required for exposures 180 sec. or longer, taken with CLOCKS=NO. This extra minute can be saved by using CLOCKS=YES, but this is not generally recommended (see section 2.6, "Serial Clocks", on page 27). If the exposure is CR-SPLIT, the readout overheads (calculated with the split exposure times) are of course doubled. There is normally no overhead time advantage in reading out a subset of the CCDs. The exception is if the WFPC2 readout occurs in parallel with the operation of a second instrument, when at least 2 minutes is required to read all 4 CCDs.

5. Spatial scans/Dithering. Spatial scans are specially designed sequences of images taken with telescope pointing changes periodically placed between successive images. The pointings in a spatial scan must either be equally spaced points on a single line, or a grid of points formed by the intersection of two sets of equally spaced parallel (but not necessarily mutually perpendicular) lines. Scans avoid the much larger alignment overheads associated with the use of POS-TARG special requirements. Dithering is the use of small spatial displacements to allow better removal of chip defects and/or the reconstruction of sub-pixel resolution. During Phase II the user will be given access to "canned" dithering routines which will allow him/her to avoid many of the tricky details involved in planning spatial scans. The overheads in these canned routines is the same as that of a user-planned spatial scan.

6. The overhead of a spatial scan is similar to that of a sequence of images taken in one alignment; however, at least one minute of overhead is required for each change in pointing. Furthermore, an extra minute of overhead is incurred at the end of the scan and typically about 1 minute of overhead is used at the beginning of the scan positioning the first image.

In summary, it is not possible to schedule exposures in different filters less than 3 minutes apart: commands to the WFPC2 are processed at spacecraft "major frame" intervals of one minute. A filter wheel may be returned to its "clear" position and another filter selected in one minute. An exposure takes a minimum of one minute, and a readout of the CCDs takes one or two minutes depending on the exposure time. Hence a simple exposure requires a minimum of 3 minutes.

Table 2.4: Instrument Overheads. The first and last exposures of an alignment contain extra overheads.

Overhead Type	Time (min.)	Overhead
First exposure	1	Major frame uncertainty, clock synchronization
First exposure	1	To put in initial filter
Per image:	1	Per filter change
Per image:	int(t)+1	t=(shutter-open time in seconds +14 seconds)/60
Per image:	1	If CLOCKS=NO (default) and exposure ≥180 sec
Per image:	1	Readout
Per image:	1	If image done in parallel with another instrument
Last exposure	1	Tape overhead
Last exposure	2	If data requested down in real-time
Last exposure	1	If a scan was done

2.8 CCD Orientation and Readout

The relation between the rows and columns for the four CCDs is shown in Figure 1.1 on page 2. Each CCD's axes are defined by a 90° rotation from the adjacent CCD. If a 4-CCD image is taken and then each subimage is displayed with rows in the "X" direction and columns in the "Y" direction, each successive display would appear rotated by 90° from its predecessor.

Table 2.5: Inner Field Edges. The CCD X,Y (Column, Row) numbers given vary at the 1-2 pixel level because of bending and tilting of the field edge in detector coordinates due to the camera geometric distortions.

Camera	Start Vignetted Field (Zero Illumination)	50% Illumination	Start Unvignetted Field (100% Illumination)
PC1	X>0 and Y>8	X>44 and Y>52	X>88 and Y>96
WF2	X>26 and Y>6	X>46 and Y>26	X>66 and Y>46
WF3	X>10 and Y>27	X>30 and Y>47	X>50 and Y>67
WF4	X>23 and Y>24	X>43 and Y>44	X>63 and Y>64

Figure 1.1 on page 2 also illustrates the projected orientation of the WFPC2 CCDs onto the sky. The beam is split between the four cameras by a

pyramid-shaped mirror in the aberrated HST focal plane. In an effort to insure images from the four CCDs can be reassembled into a single image without gaps, there is a small overlap region on the sky between each CCD and its neighbors (see also Figure 3.11 on page 62). On the CCDs this region appears as a blank "shadow" region along the X~0 and Y~0 edges of each CCD; the exact limits of this region are given in Table 2.5 for each CCD. Because the OTA beam is aberrated at the pyramid mirror, the edges of the shadow region are not sharp, but instead there is a gradual transition from zero to full illumination on each CCD. The width of this vignetted region is essentially that of the aberrated OTA beam (~5″). Table 2.5 gives approximate limits of this vignetted region on each CCD. Note that astronomical sources in the vignetted region are imaged onto two or more CCDs.

The WFPC2 has two readout formats, namely full single pixel resolution (FULL Mode), and 2x2 pixel summation (AREA Mode which is obtained by specifying the optional parameter SUM=2x2 as described in the Proposal Instructions). Each line of science data is started with two words of engineering data, followed by 800 (FULL) or 400 (AREA) 16-bit positive numbers as read from the CCDs (with 12 significant bits). In FULL Mode the CCD pixels are followed by 11 "bias" words ("over-clocked" pixels), yielding a total of 813 words per line for 800 lines. In AREA Mode, there are 14 bias words giving a total of 416 words per line for 400 lines. Either pixel format may be used to read out the WFC or PC. These outputs are reformatted into the science image and extracted engineering data files during processing in the HST ground system prior to delivery to the observer.

The advantage of the AREA Mode (2x2) on-chip pixel summation is that readout noise is maintained at 5 e^- RMS for the summed (i.e., larger) pixels. In addition, more images will fit onto the spacecraft tape recorder. This pixel summation is useful for some photometric observations of extended sources particularly in the UV. Note, however, that cosmic ray removal is more difficult in AREA Mode.

The readout direction along the columns of each CCD is indicated by the small arrows near the center of each camera field in Figure 1.1 on page 2 (see also Figure 3.11 on page 62). Columns and rows are parallel and orthogonal to the arrow, respectively. Each CCD is read out from the corner nearest the center of the diagram, with column (pixel) and row (line) numbers increasing from the diagram center. In a saturated exposure, blooming will occur almost exclusively along the columns because of the MPP operating mode of the CCDs. Diffraction spikes caused by the Optical Telescope Assembly and by the internal Cassegrain optics of the WFPC2 are at 45° to the edges of the CCDs. Unless specified otherwise in the Phase 2 proposal, the default pointing position when all 4 CCDs are used is on WF3, approximately 10″ along each axis from the origin.

Observations which require only the field-of-view of a single CCD are best made with the target placed near the center of a single CCD rather than near the center of the 4 CCD mosaic. This results in a marginally better point spread function, and avoids photometric, astrometric, and cosmetic problems in the vicinity of the target caused by the overlap of the cameras. Even so, for such observations the default operational mode is to read out all four CCDs. This policy has resulted in serendipitous discoveries, and sometimes the recovery of useful observations despite pointing or coordinate errors.

On the other hand, any combination of 1, 2 or 3 CCDs may be read out in numerical order (as specified in the Proposal Instructions). This partial readout capability is not generally available to GOs, although it can be used if data volume constraints mandate it, after discussion with the WFPC2 instrument scientists. It does not result in a decrease in the readout overhead time but does conserve limited space on the HST on-board science tape recorder. The capacity of the present science tape recorder is slightly over 7 full (4-CCD) WFPC2 observations and 18 single CCD WFPC2 observations on a single tape recorder side (of two). Switching sides of the tape recorder without a pause will result in the loss of part of a single CCD readout. Since an interval of about 30 minutes must normally be allowed for the tape recorder to be copied to the ground, readout of only a subset of the WFPC2 CCDs, or use of AREA mode, can be advantageous when many frames need to be obtained in rapid succession. Note, however, that the Solid State Recorder planned for installation during the 1997 Service Mission is capable of hold well over one hundred 4-CCD WFPC2 images. This capability should be phased-in during Cycle 7, and will lead to relaxation of the above data rate restrictions for Cycle 7 proposals.

Multiple exposures may be obtained with or without interleaved spacecraft repointings and filter changes without reading the CCDs (READ=NO). These would then be followed by a readout (READ=YES). Note that WFPC2 must be read out at least once per orbit.

2.9 Calibration Channel

An internal flat field system provides reference flat field images over the spectral range of WFPC2. These are provided by a "calibration channel" optical system mounted outside the main shroud of WFPC2. The system consists of a series of lamps and diffusers, and a flip mirror which directs the beam into the WFPC2 entrance aperture. The lamp set contains Tungsten incandescent lamps with spectrum shaping glass filters and a Deuterium UV lamp. The flat field illumination pattern is fairly uniform for wavelengths beyond about 1600Å. Short of 1600Å the flat field is distorted due to refractive MgF_2 optics. In practice, the flat fields used routinely to calibrate WFPC2 data have been generated by combining flats taken with an external stimulus in thermal vacuum testing with Earth "streak" (unpointed) flats to give the low frequency terms in the OTA illumination pattern. The calibration channel is used primarily to check for internal instrumental stability.

CHAPTER 3: Optical Filters

In This Chapter...

Introduction / 35
Choice of Broad Band Filters / 40
Linear Ramp Filters / 40
Redshifted [OII] Quad Filters / 49
Polarizer Quad Filter / 50
Methane Quad Filter / 53
Wood's Filters / 54
Red Leaks in UV Filters / 57
Apertures / 60

3.1 Introduction

A set of 48 filters are included in WFPC2 with the following features:

1. It approximately replicates the WF/PC-1 "UBVRI" photometry series.
2. The broad-band filter series extends into the far UV.
3. There is a Strömgren series.
4. A Wood's filter is available for far-UV imaging without a red leak.
5. There is a 1% bandpass linear ramp filter series covering 3700-9800Å.
6. The narrow-band series is uniformly specified and well calibrated.

The filters are mounted in the Selectable Optical Filter Assembly (SOFA) between the shutter and the reflecting pyramid. The SOFA contains 12 filter wheels, each of which has 4 filters and a clear "home" position. A listing of all simple optical elements in the SOFA mechanism, and the location of each element (by wheel number 1-12, and position 1-4) is given in Table 3.1. Wheel number 1 is located closest to the shutter. The categories of simple filters (F) are long-pass (LP), wide (W), medium (M), and narrow (N). Most of these filters are either flat single substrates or sandwiches.

The filter complement includes two solar blind Wood's filters, F160AW and F160BW. F160BW is used in all science observations because the other filter has some large pinholes that lead to significant red leak.

In addition to the above complement of broad and narrow-band filters, WFPC2 features a set of three specialized quadrant (quad or Q) filters in which each quadrant corresponds to a facet of the pyramid, and therefore to a distinct camera relay. There is one quad containing four narrow-band, redshifted [OII] filters with central wavelengths from 3763Å to 3986Å, one quad with four polarizing elements (POL) with polarization angles, 0°, 45°, 90° and 135°, and one quad with four methane (CH4) band filters with central wavelengths from 5433Å to 8929Å. The polarizer quad filter can be crossed with any other filter over the wavelength range from 2800Å to 8000Å, with the exception of the Methane Quad and Redshifted [OII] Quad which share the same wheel. The SOFA also contains four linearly variable narrow-band ramp (FR) filters (in the twelfth wheel - closest to the focus). The quad and ramp filters are listed in Table 3.2.

In Table 3.1 and Table 3.2, each of the type "A" filters is equivalent to inserting 5 mm of quartz in terms of optical path length, with compensation for wavelength such that focus is maintained on the CCDs. A configuration with no filters in the beam results in out-of-focus images and generally will not be used. With the exception of the quad polarizer and blocking (Type "B") filters, all filters are designed to be used alone. Type "B" filters introduce no focus shift, so they can be used in combination with any type "A" filter. All combinations where the number of type "A" filters is not unity will result in out-of-focus images. The image blur resulting from two or zero type "A" filters at visible wavelengths is equivalent to 2.3 mm defocus in the F/24 beam, which corresponds to 1/5 wave RMS of defocus at 6328Å, and a geometrical image blur of 0.34″. While this is a large defocus, the images are still of very high quality compared to seeing limited images. Some such combinations may be scientifically attractive. For example, the Wood's filter may be crossed with another UV filter to provide a solar blind passband (although the efficiency will be low).

The mean wavelength, $\bar{\lambda}$, is similar to that defined in Schneider, Gunn and Hoessel (Ap. J. 264, 337). The width is the FWHM of a Gaussian filter with the same second moment, and is reasonably close to the FWHM. The values tabulated here do not include the CCD DQE or the transmission of the OTA or WFPC2 optics (as given in Figure 2.4). In Chapter 6, the corresponding quantities are given including the effect of the other optical elements and the CCD DQE.

Figure 3.1 summarizes the normalized transmission curves for the simple filters and narrow-band quad filters. It does not include curves for the polarizing quad, or the linear ramp filters which are documented in sections 3.2 and 3.4 respectively. Individual filter transmission curves are shown in the Appendix starting on page 201. Figure 3.1 divides the filters into the following groups:

1. Long pass filters designed to be used in combination with another filter.
2. Wide bandpass filters with FWHM ~25% of the central wavelength.
3. Approximations to the UBVRI sequence, generally with wider bandpasses, designed for use on faint sources.
4. A photometric set of approximations to UBVRI passbands (see Harris et al. 1991, A.J. 101, 677). Note, however, that the WFPC2 UBVRI series is not the Johnson-Cousins photometric series, neither is it identical with the WF/PC-1 series. See Chapter 6 for detailed comparisons.

Table 3.1: WFPC2 Simple Filter Set. The effective wavelength, width, and transmission quoted are defined precisely in Chapter 6, but here are quoted without the system (OTA_WFPC2) response.

Name	Type	Wheel	Slot	Notes	In WF/PC-1?	$\bar{\lambda}$(Å)	$\Delta\bar{\lambda}$(Å)	Peak T (%)	Peak λ (Å)
F122M	A	1	4	H Ly α - Red Leak	Y	1292	263.5	18.9	1240
F130LP	B	2	1	CaF2 Blocker (zero focus)	N	3847	5568.1	94.7	4344
F160AW	A	1	3	Woods A - redleak from pinholes	N	1471	457.2	10.1	1403
F160BW	A	1	2	Woods B	N	1471	457.2	10.1	1403
F165LP	B	2	2	Suprasil Blocker (zero focus)	N	4327	5505.7	92.1	3109
F170W	A	8	1	-	N	1689	434.9	30.3	1667
F185W	A	8	2	-	N	1907	302.9	23.7	1849
F218W	A	8	3	Interstellar feature	N	2136	355.9	21.3	2091
F255W	A	8	4	-	N	2557	408.2	15.5	2483
F300W	A	9	4	Wide U	N	2924	727.6	51.8	2760
F336W	A	3	1	WFPC2 U, Strömgren *u*	Y	3327	370.7	80.3	3447
F343N	A	5	1	Ne V	N	3430	24.3	19.7	3433
F375N	A	5	2	[OII] 3727 RS	Y	3736	26.2	17.2	3736
F380W	A	9	1	-	N	3934	694.7	65.6	3981
F390N	A	5	3	CN	N	3889	45.3	37.8	3886
F410M	A	3	2	Strömgren *v*	N	4088	146.9	70.1	4098
F437N	A	5	4	[OIII]	Y	4369	25.2	52.0	4368
F439W	A	4	4	WFPC2 B	Y	4292	464.4	67.3	4176
F450W	A	10	4	Wide B	N	4445	925.0	92.4	5061
F467M	A	3	3	Strömgren *b*	N	4682	171.5	75.3	4728
F469N	A	6	1	He II	Y	4695	24.9	52.4	4699
F487N	A	6	2	H β	Y	4865	25.8	58.6	4863
F502N	A	6	3	[OIII]	Y	5012	26.8	63.8	5009
F547M	A	3	4	Strömgren *y* (but wider)	Y	5454	486.6	91.3	5361
F555W	A	9	2	WFPC2 V	Y	5252	1222.5	94.8	5151
F569W	A	4	2	F555W generally preferred[a]	Y	5554	965.8	94.2	5309
F588N	A	6	4	He I & Na I (NaD)	Y	5892	49.1	91.5	5895
F606W	A	10	2	Wide V	Y	5843	1578.7	98.3	6183
F622W	A	9	3	-	Y	6157	935.4	95.6	6034
F631N	A	7	1	[OI]	Y	6306	30.8	85.7	6302
F656N	A	7	2	Hα	Y	6562	22.0	77.9	6561
F658N	A	7	3	[NII]	Y	6590	28.5	79.7	6592
F673N	A	7	4	[SII]	Y	6733	47.2	87.0	6733
F675W	A	4	3	WFPC2 R	Y	6735	889.4	97.9	6796
F702W	A	10	3	Wide R	Y	6997	1480.7	98.5	6539
F785LP	A	2	3	F814W generally preferred[a]	Y	9366	2094.7	96.0	9960
F791W	A	4	1	F814W generally preferred[a]	Y	8006	1304.2	99.7	8081
F814W	A	10	1	WFPC2 I	Y	8269	1758.0	98.4	8386
F850LP	A	2	4	-	Y	9703	1669.5	95.5	10026
F953N	A	1	1	[SIII]	N	9546	52.5	95.6	9528
F1042M	A	11	2	-	Y	10443	610.9	95.2	10139

a. Filters F555W and F814W are generally preferred, as they are part of the “standard” WFPC2 filter set, and will tend to have slightly better photometric calibration. See “Choice of Broad Band Filters” on page 40.

Table 3.2: WFPC2 Quad and Ramp Filters. Segments of the UV and CH4 quads are labeled here by their usual physical designations (A, B, C, and D); see following sections for filter and aperture names which are to be used in writing Phase II proposal. The quad polarizer is represented for both parallel and perpendicular polarization to its polarization direction, which is different in each quadrant.

Physical Name	Type	Wheel	Slot	Notes	In WF/PC-1	$\bar{\lambda}$(Å)	$\Delta\bar{\lambda}$(Å)	Peak T (%)	Peak λ (Å)
FQUVN-A	A	11	3	Redshifted [OII] 375	N	3767	73.4	24.0	3769
FQUVN-B	A	11	3	Redshifted [OII] 383	N	3831	57.4	30.5	3827
FQUVN-C	A	11	3	Redshifted [OII] 391	N	3915	59.3	38.9	3908
FQUVN-D	A	11	3	Redshifted [OII] 399	N	3993	63.6	43.4	3990
FQCH4N-A	A	11	4	CH4 543	N	5433	38.0	83.8	5442
FQCH4N-B	A	11	4	CH4 619	N	6193	44.0	83.7	6202
FQCH4N-C	A	11	4	CH4 727	N	7274	51.0	89.7	7279
FQCH4N-D	A	11	4	CH4 892	N	8929	64.0	91.2	8930
POLQ_par	B	11	1	Pol angle 0˚,45˚,90˚,135˚	N	5427	5797.6	90.8	10992
POLQ_per	B	11	1	Pol angle 0˚,45˚,90˚,135˚	N	7922	6653.4	89.7	10992
FR418N	A	12	1	3700-4720	N	W	W/75	~20-50	W
FR533N	A	12	2	4720-6022	N	W	W/75	~40-50	W
FR680N	A	12	3	6022-7683	N	W	W/75	~60-80	W
FR868N	A	12	4	7683-9802	N	W	W/75	~70-85	W

5. Medium bandpass filters with FWHM ~10% of the central wavelength, including an approximation to the Strömgren photometric series.
6. Narrow bandpass filters for isolating individual spectral lines or bands.
7. Redshifted [OII] and CH4 narrow bandpass quad filters.

Note that the UV filters have some degree of "red leak," which is quantified in Chapter 6 where the system response is included.

A passband calibration is maintained in the calibration database system (CDBS). It has been updated following on orbit calibrations. The ground based calibration of the narrow-band filters' central wavelengths has not been corrected for temperature effects and is therefore accurate to about 2Å. Because of this, it is not advisable to place narrow emission lines at the half power points of such filters and expect to predict the throughput to high accuracy. The standalone software package XCAL, or SYNPHOT running under IRAF, can be used to access these calibrations which are available on the Institute's WWW page.

Figure 3.1: Summary of Normalized Filter Curves.

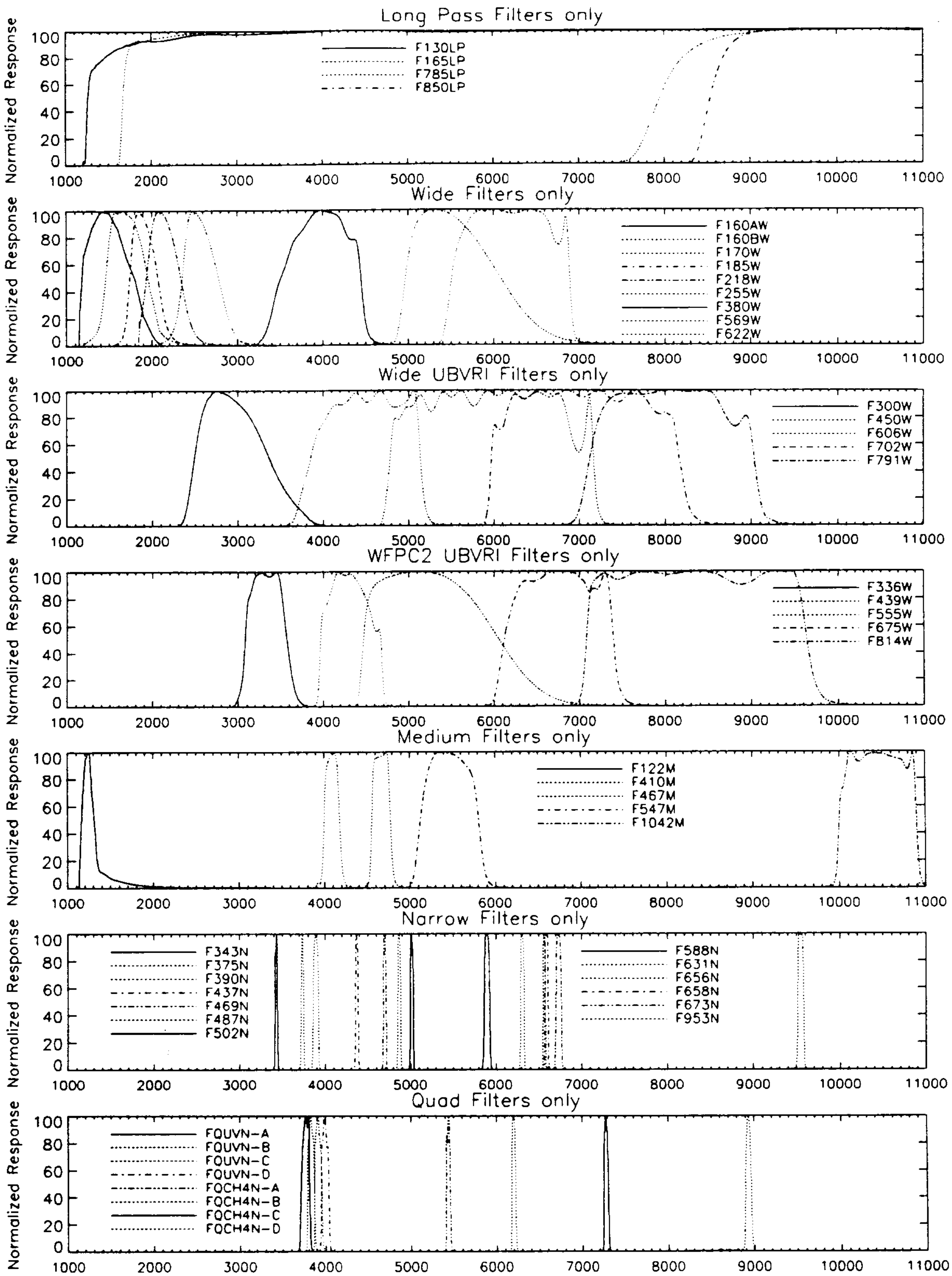

3.2 Choice of Broad Band Filters

A number of different choices are possible on WFPC2 in order to approximate the Johnson-Cousins system often used in ground based observing. These choices differ in throughput, wavelength fidelity, color transformability, and cosmetics. The HST science program as a whole benefits if a standard set can be agreed upon by the community for broad band photometry. This will allow theoretical isochrones and other models to be published in the standard system, and allow ready comparison of the results from different observers. Furthermore, although all filters will be calibrated photometrically and with flat fields, a core set must be chosen for monitoring the instrument both photometrically and in imaging performance. There was a substantial consensus between the accepted Cycle 4 GO programs and the WF/PC-1 and WFPC2 science teams that F336W, F439W, F555W, F675W, and F814W should be the preferred set to approximate the Johnson Cousins U, B, V, R, I passbands. These filters form the basis for the WFPC2 broad band photometric system. As will be seen from the figures in Section 8.8 (page 172), the preferred set is accurately transformable with the exception of the U bandpass.

On the other hand, there are situations where concerns such as maximum throughput must override the above arguments. For example, filters F300W, F450W, F606W, and F814W were chosen for the Hubble Deep Field (HDF), due to their wider bandpasses.

3.3 Linear Ramp Filters

The linear ramp filters are designed for narrow-band absorption and emission line imaging of moderately extended objects. Each filter is divided into four parallel strips where the central wavelength across each strip varies by approximately 6%. Each CCD pixel is mapped to a unique central wavelength with a FWHM bandwidth of approximately 1.3% of the central wavelength. The maximum size of an object which can be imaged at a given wavelength is approximately 13″ and is determined by the width of the strips and the image size at the filter. The cumulative wavelength range of the four linear ramp filters is 3710Å to 9762Å. Originally intended for a four WFC configuration, the linear ramp filters require partial rotation of the SOFA wheels to +15°, -18° and -33° from their nominal positions, to recover wavelength regions which would fall on the PC camera or otherwise be lost. There will be vignetting at some wavelengths for these partial rotations.

3.3.1 Spectral Response

A JPL Memorandum (DFM #2031, 1992) gives the results of a prediction scheme to locate and quantify the passbands of the four WFPC2 ramp filters, FR418N, FR533N, FR680N and FR866N. The results are summarized here.

Laboratory (room temperature) measurements of the passbands of the four ramp filters were made at five equally spaced intervals on each of the four ramp stripes on each filter for a total of 80 passband measurements. The laboratory measurements were made with a narrow beam and were then integrated over an annular area of the filter to simulate the beam profile. The radius of the beam is 3.7 mm, or 13″. The integration was carried out by assuming the nominal linear shift in wavelength with position, and that no significant changes in the passband shape occur across the beam. The integration makes the shape of the passband quite symmetrical.

The resulting spectral response can be fitted to within a few percent with a Munson function:

$$T = T_0 / \{ 1 + (1-a)x^2 + a(1-b)x^4 + ab(1-c)x^6 + abcx^8 \}$$

where a, b and c are shape parameters, and $0 \le (a,b,c) \le 1$; T_0 is the peak transmission of the passband, $T=T_0$ at $x=0$; x is related to wavelength λ by $x=(\lambda-\lambda_0)/H$, $T=T_0/2$ at $x=1$ (so H is the half width at half maximum).

The parameters, (λ_0, T_0, H, a, b, c) were then fitted to polynomial functions of position Y (which starts at 0 inches at the lower wavelength edge of each strip) to predict the filter response for areas of the filters between the tested points. Good quadratic fits are available for all the parameters except for T_0 which requires a cubic. The results are given in Tables 3.3 through 3.6, which give the polynomial fit coefficients for the ramp filter parameters. The table entries, except for the first line, are used as parameter=A_0+A_1Y+A_2Y_2+A_3Y_3. The short wavelength side of the filter is opposite for alternate ramps. The first line in each table gives the Y position as a function of λ. If the polynomial fit predicts a, b, or $c < 0$ or > 1 then the quantities are set to 0 or 1 respectively.

Use of these fits should be restricted to objects near the center of the ramp, otherwise the beam will combine light from adjacent ramps. The fit should also not be used within 13″ of the end of the ramp. There is enough wavelength overlap between ramps that the extreme ends need not be used, except at the very lowest and highest wavelengths. Figure 3.2 shows the fit parameter T_0 as a function of λ_0 for all 16 ramp filter strips. Figure 3.3 shows $2H/\lambda_0$.

Figure 3.2: Ramp Filter Peak Transmission. The four line types correspond to the four different filters (each containing four ramps).

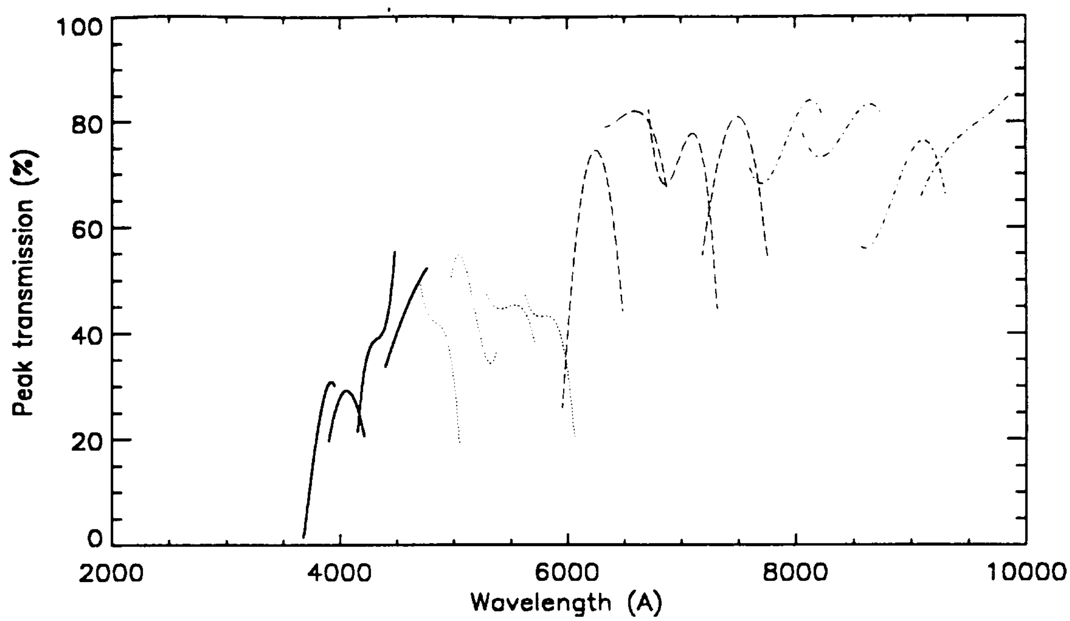

Figure 3.3: Ramp Filter Dimensionless Widths.

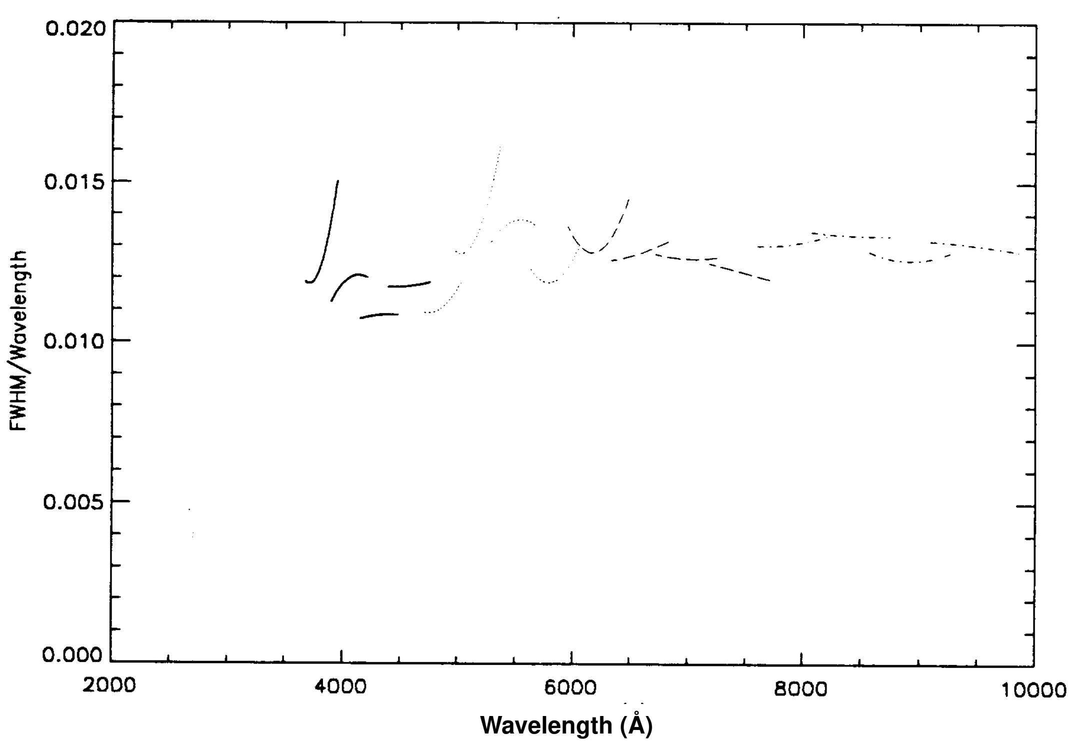

Table 3.3: Ramp Filter FR418N Parameters.

Quantity	A0	A1	A2	A3
Ramp 1 Position	-26.1083	.00713888	.0000	
Wavelength	3657.7	138.7	.6178	
Peak transmission	-.01667	.2188	.04138	-.03489
Half width at half max	21.95	-.8347	2.143	
a	.2120	.002857	.002596	
b	1.181	-.8138	.3535	
c	.3301	-.3715	.3825	
Ramp 2 Position	-24.2554	.00625704	.0000	
Wavelength	3876.9	158.6	.5472	
Peak transmission	.1660	.2288	-.1080	.004005
Half width at half max	21.50	3.315	-.7079	
a	.1592	-.003687	-.0008497	
b	.7938	.2355	-.09124	
c	.9306	.01366	.007458	
Ramp 3 Position	-24.7145	.00598254	.0000	
Wavelength	4130.5	168.8	-.7389	
Peak transmission	.1352	.6200	-.5226	.1529
Half width at half max	22.09	1.306	-.1181	
a	.2300	.05586	-.03044	
b	1.096	-.3185	.1396	
c	1.276	-1.279	.5721	
Ramp 4 Position	-23.4440	.00536340	.0000	
Wavelength	4371.3	185.8	.2913	
Peak transmission	.3189	.1287	-.01160	-.001712
Half width at half max	25.62	1.015	.1161	
a	.3123	-.2055	.09535	
b	.9222	.1167	-.04673	
c	1.033	-.1356	.05660	

Table 3.4: Ramp Filter FR533N Parameters.

Quantity	A0	A1	A2	A3
Ramp 1 Position	-26.7670	.00572115	.0000	
Wavelength	4677.7	177.3	-1.125	
Peak transmission	.5450	-.3612	.3623	-.1281
Half width at half max	25.67	.3168	.8873	
a	-.009839	.4644	-.2039	
b	.31511	.9473	-.4516	
c	-.3379	2.788	-1.346	
Ramp 2 Position	-24.6600	.00498393	.0000	
Wavelength	4948.4	199.2	.6484	
Peak transmission	.4546	.4188	-.5456	0.1548
Half width at half max	32.10	-1.204	3.171	
a	.1678	-.02726	.09521	
b	.9345	.1935	-.1224	
c	.9571	.02919	-.009393	
Ramp 3 Position	-24.5038	.00465985	.0000	
Wavelength	5257.3	217.9	-1.481	
Peak transmission	.4944	-.1714	.1890	-0.0631
Half width at half max	34.03	5.078	-1.347	
a	.3851	-.06264	.003163	
b	.5605	.6642	-.2751	
c	.9665	.05543	-.03654	
Ramp 4 Position	-25.5182	.00455886	.0000	
Wavelength	5596.9	220.9	-.6938	
Peak transmission	.5058	-.2715	.3203	-.1230
Half width at half max	35.06	-2.856	2.382	
a	.06553	.2253	-.08275	
b	1.043	-.1190	.02889	
c	1.162	-.4910	.2059	

Table 3.5: Ramp Filter FR680N Parameters.

Quantity	A0	A1	A2	A3
Ramp 1 Position	-21.8962	.00370137	.0000	
Wavelength	5916.0	269.4	.3460	
Peak transmission	.1198	1.005	-.4015	-.00162
Half width at half max	41.50	-5.873	4.038	
a	.1743	-.05050	.06481	
b	.8320	.3326	-.1858	
c	.9682	-.09110	.05122	
Ramp 2 Position	-22.6919	.00360750	.0000	
Wavelength	6290.8	275.6	.7184	
Peak transmission	.7918	-.02034	.1086	-.05945
Half width at half max	39.48	2.120	.3703	
a	.05596	.3034	-.1333	
b	1.017	-.27026	.04560	
c	.7244	.8326	-.5107	
Ramp 3 Position	-22.0719	.00330755	.0000	
Wavelength	6673.5	301.6	.3321	
Peak transmission	.9494	-1.008	1.161	-.3777
Half width at half max	42.81	.8193	.4269	
a	.1038	.09020	-.02747	
b	.8415	.3045	-.1930	
c	1.017	-.1732	.07463	
Ramp 4 Position	-24.7447	.00346462	.0000	
Wavelength	7141.9	289.3	-.2999	
Peak transmission	.4823	.4479	-.07484	-.05868
Half width at half max	44.72	.8952	-.0756	
a	.1612	-.01167	.01355	
b	.2708	1.077	-.4757	
c	.9941	-.02694	.01685	

Table 3.6: Ramp Filter FR868N Parameters.

Quantity	A0	A1	A2	A3
Ramp 1 Position	-23.2685	.00308029	.0000	
Wavelength	7555.5	320.4	1.906	
Peak transmission	.7524	-.3328	.4543	-.1343
Half width at half max	49.32	1.742	.4914	
a	.2958	-.3877	.2465	
b	1.321	-.9156	.3666	
c	.3762	1.668	-.9499	
Ramp 2 Position	-22.9766	.00286673	.0000	
Wavelength	8014.3	350.5	-.7500	
Peak transmission	.8204	-.3368	.3815	-.1057
Half width at half max	54.17	1.579	.2196	
a	.05832	.7525	-.3625	
b	.4582	.8433	-.4350	
c	.6422	.3247	-.1593	
Ramp 3 Position	-22.6085	.00265657	.0000	
Wavelength	8510.7	375.6	.3706	
Peak transmission	.5817	-.1920	.4517	-.1627
Half width at half max	55.19	-.7459	1.433	
a	.5422	-.2444	.03545	
b	1.420	-1.176	.4814	
c	.4257	-.2522	.1777	
Ramp 4 Position	-23.2142	.00256976	.0000	
Wavelength	9034.3	387.2	.8722	
Peak transmission	.6241	.2403	-.1230	.02829
Half width at half max	59.69	2.167	-.1996	
a	.2376	-.01879	-.00864	
b	.9670	.02456	-.00477	
c	.7829	.03750	.02393	

3.3.2 Target Locations

In Figures 3.4 and 3.5 we show the correspondence between central wavelength and location in the focal plane for the nominal and rotated filter positions. The selection of filter and aperture for the linear ramp filters is transparent to the user who is required only to specify the linear ramp filter name LRF and a central wavelength. Each central wavelength is assigned to a unique filter and CCD location.

Following on-orbit testing of WFPC2 a revised table of linear ramp filter wavelengths has been compiled and is shown in Table 3.7. For each wavelength listed, there is a minimum 10″ diameter unvignetted field-of-view. Some wavelengths can be obtained with several different settings of the ramps, however, for simplicity, the redundant wavelengths have been removed from the table. Note that this table supports observation with the PC and a new $+15^{\circ}$ rotation of the filter wheel. Table 3.8 lists wavelengths which are available, but with some compromise in data quality, so as to avoid gaps in wavelength coverage. Most of these wavelengths are observed slightly off the central wavelength of the passband. This implies a slightly reduced throughput (see estimates of the light reduction in the table), and some additional difficulties in flattening the data to remove variations in the passband across the target. A few other wavelengths are observed slightly off the unvignetted centerline of the ramps, and these are indicated by note "FOV" in Table 3.8. Again, this vignetting will present some additional complications when calibrating the data. Further details regarding the ramp filter wavelengths and apertures will be made available in a separate instrument science report.

We note that an interactive tool is available on the WFPC2 WWW pages which will compute target locations for LRF observations. The user inputs either the central wavelength or the target location in the field-of-view, and the other quantity is returned.

3.3.3 LRF Photometric Calibration

As of this writing, the preferred method of flat fielding LRF data is to use a narrow band flat observed nearby in wavelength. This will remove pixel-to-pixel effects, as well as effects of distortion and vignetting in the cameras, while avoiding the complications of pinholes on the LRFs and spurious variations due to the spectrum of the flat field light source.

Conversion of counts to source flux is best achieved by using the SYNPHOT synthetic photometry package. An LRF filter setting is simply specified by including "LRF#*xxxx*" in the OBSMODE, where *xxxx* is the central wavelength specified on the Phase II proposal.

Figure 3.4: FR418N and FR533N Wavelength Mapping.

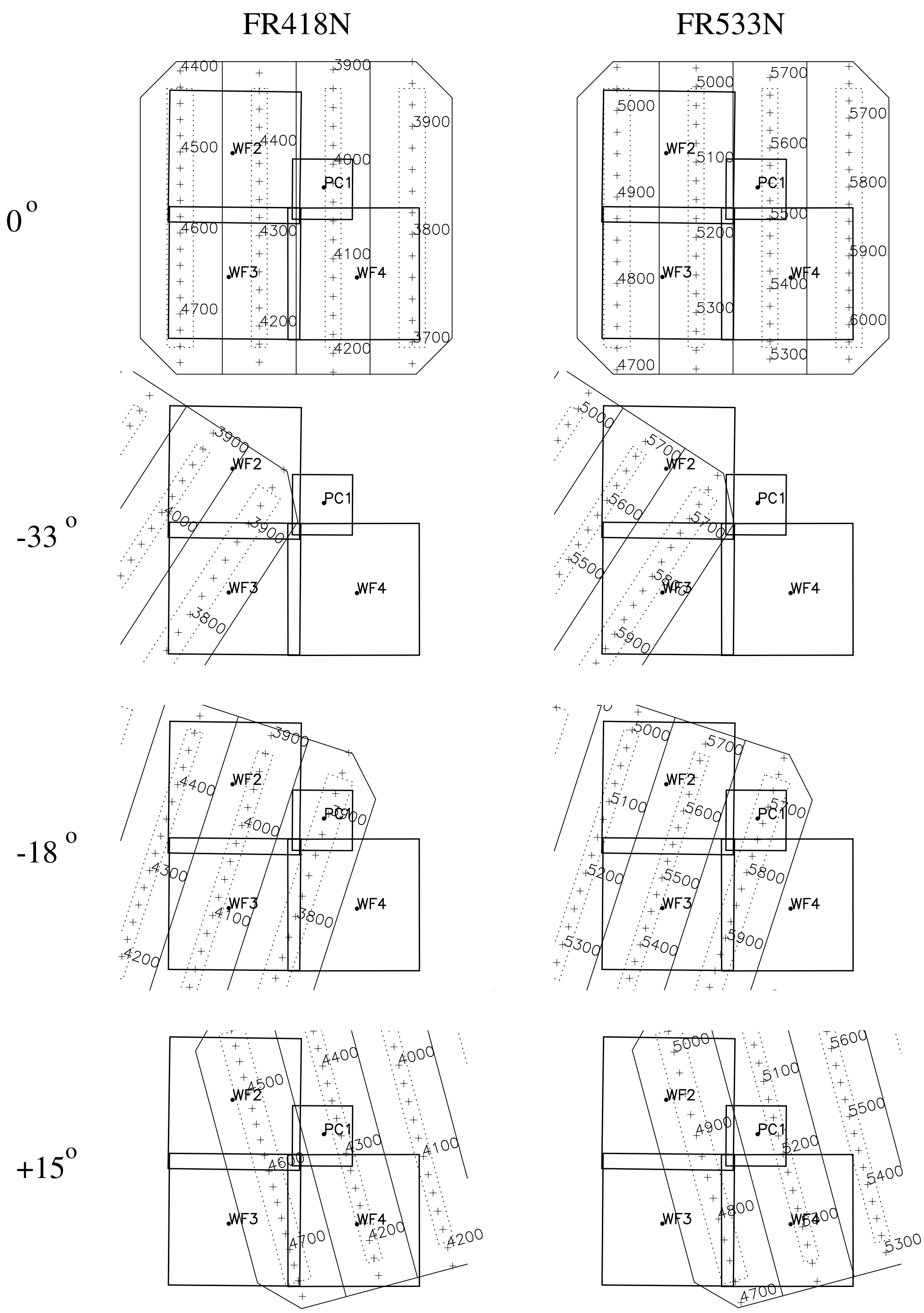

Figure 3.5: FR680N and FR868N Wavelength Mapping.

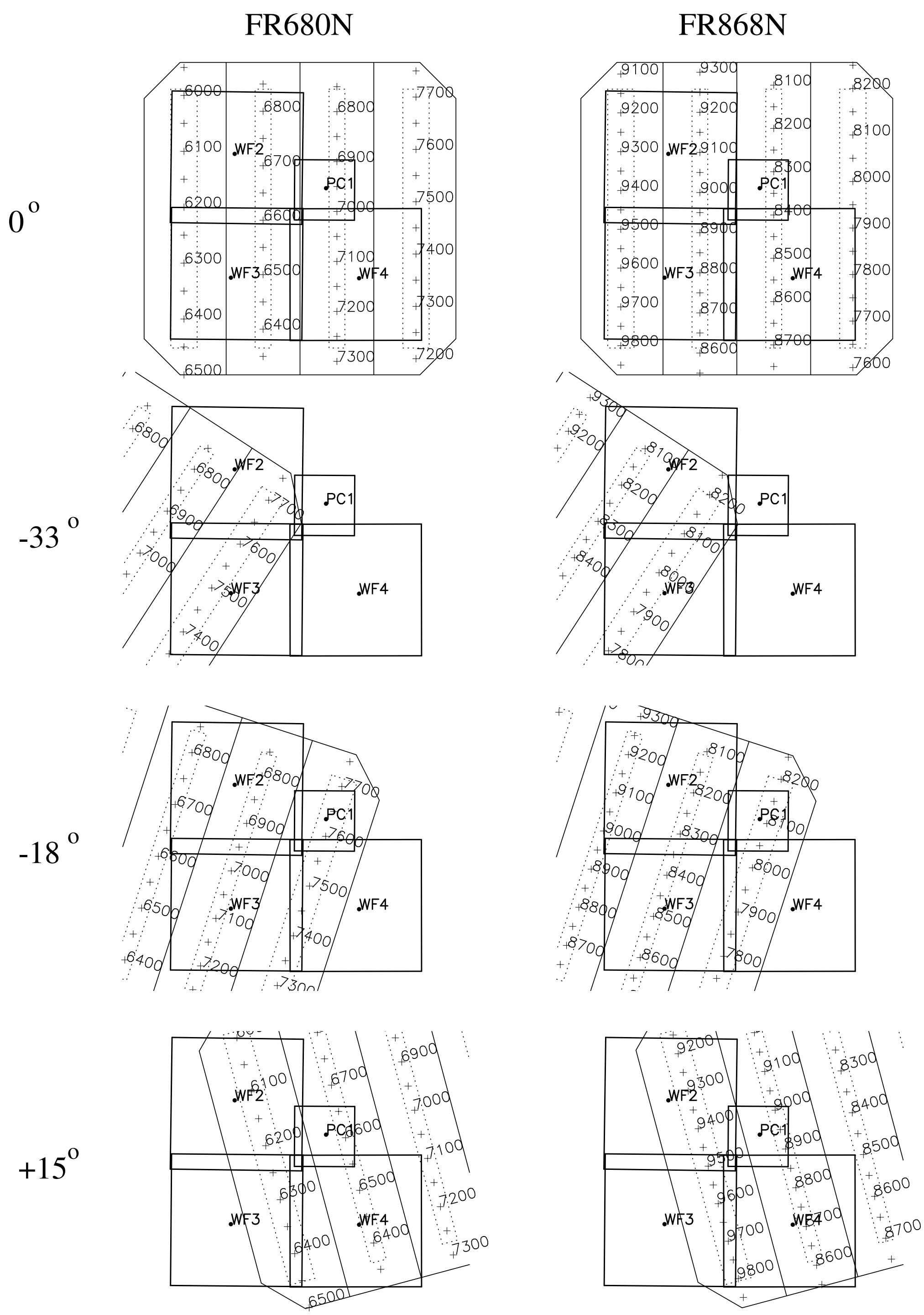

Table 3.7: Aperture Locations and Wavelengths for Ramp Filters.

Start (Å)	End (Å)	Filter	CCD / Aperture	x1 (pix)	y1 (pix)	x2 (pix)	y2 (pix)
3710	3800	FR418N	WF4-FIX	750	736.8	161 .5	737.7
3800	3878	FR418N33	WF3-FIX	669.5	559.2	395.1	128.9
3881	3907	FR418N18	PC1-FIX	402.3	225	515.4	579.5
3907	3929	FR418N33	WF2-FIX	128.4	286.7	250.1	209.9
3929	4008	FR418N18	WF2-FIX	562.7	233	130.1	367.1
4008	4038	FR418N	PC1-FIX	541.3	632.7	543.3	256.5
4038	4100	FR418N18	WF3-FIX	425.3	130.8	532 4	469.9
4100	4177	FR418N	WF4-FIX	309	276.2	750.3	275.5
4186	4210	FR418P15	WF4-FIX	596.5	515.9	469.4	482.1
4210	4308	FR418N	WF3-FIX	248.2	665.9	252.7	128.5
4308	4337	FR418P15	PC1-FIX	690.2	264.6	598.4	599.9
4337	4446	FR418N	WF2-FIX	127.9	247.6	725.4	255.7
4446	4550	FR418N	WF2-FIX	691.7	716.2	180.6	709.2
4550	4571	FR418P15	WF2-FIX	230	253.8	130.7	225.8
4593	4720	FR418N	WF3-FIX	713.7	125.6	708.5	749.9
4746	4863	FR533N	WF3-FIX	689.3	748.9	694.4	135.5
4884	4900	FR533P15	WF2-FIX	128.3	205.1	209	227.9
4900	5013	FR533N	WF2-FIX	153.6	689.6	745.9	697.7
5013	5020	FR533N18	WF2-FIX	693.4	642.4	662.9	651.8
5020	5153	FR533N	WF2-FIX	737.3	236.6	130	228.4
5153	5176	FR533P15	PC1-FIX	637.9	614.9	698.6	393.3
5188	5310	FR533N	WF3-FIX	233.5	127.4	228.8	684.7
5310	5335	FR533P15	WF4-FIX	482.8	505.5	593.1	534.9
5339	5450	FR533N	WF4-FIX	750.9	294.7	277.2	295.5
5450	5528	FR533N18	WF3-FIX	504.4	445.3	404.1	127.6
5528	5566	FR533N	PC1-FIX	585.3	277.5	583.4	632.3
5566	5671	FR533N18	WF2-FIX	124.1	348.8	552.3	216.1
5671	5700	FR533N33	WF2-FIX	224.8	203.2	122.3	267.7
5700	5741	FR533N18	PC1-FIX	558.8	577	444.9	220.1
5743	5910	FR533N33	WF3-FIX	370.8	126.5	745.9	714.9
5910	6007	FR533N	WF4-FIX	333.8	747.6	738.8	746.9
6007	6192	FR680N	WF2-FIX	750.3	706.9	122.9	698.4
6192	6208	FR680P15	WF2-FIX	177.1	228.4	124.9	213.6
6238	6409	FR680N	WF3-FIX	703.6	128.1	698.8	708.2
6409	6584	FR680N	WF3-FIX	237.8	705.6	242.6	127
6590	6631	FR680P15	PC1-FIX	699.1	315.3	620.9	601.2
6631	6800	FR680N	WF2-FIX	125.9	237.5	684.5	245.1
6800	6921	FR680N18	WF2-FIX	480.1	248	129.9	356.6
6921	6976	FR680N	PC1-FIX	563.3	639.2	565.3	274.6
6976	7061	FR680N18	WF3-FIX	413.2	126	490.8	371.7
7061	7241	FR680N	WF4-FIX	203	286.4	748.3	285.6
7251	7420	FR680N	WF4-FIX	749.6	743.5	213.3	744.3
7420	7600	FR680N33	WF3-FIX	688.9	608.4	381.6	126.4
7605	7658	FR680N18	PC1-FIX	427	230	538.9	580.6
7658	7690	FR680N33	WF2-FIX	126.2	276.1	212.1	222
7690	7830	FR868N	WF4-FIX	711.5	751.3	316.5	751.9
7830	8072	FR868N33	WF3-FIX	728.2	705.8	360.9	129.7
8077	8140	FR868N18	PC1-FIX	471.5	231	589.7	601.5
8140	8300	FR868N18	WF2-FIX	527.6	213.2	126.2	337.6
8300	8362	FR868N	PC1-FIX	605.4	644.1	607.3	287.9
8362	8460	FR868N18	WF3-FIX	393.1	126.1	470.6	371.7
8460	8661	FR868N	WF4-FIX	196.9	305.7	724.7	304.9
8661	8910	FR868N	WF3-FIX	218.3	731.6	223.4	125.3
8945	8980	FR868P15	PC1-FIX	701.1	467.5	651.9	647.3
8980	9200	FR868N	WF2-FIX	142.7	218.5	678.2	225.8
9200	9415	FR868N	WF2-FIX	668.4	686.5	162.2	679.6
9415	9456	FR868P15	WF2-FIX	219.9	220.5	127	194.2
9501	9762	FR868N	WF3-FIX	684.3	135.4	679.2	750.2

Table 3.8: Vignetted Wavelengths for Ramp Filters. The right column gives the maximum throughput reduction (in %) for these settings where the target must be placed away from the optimal location on the filter glass. "FOV" denotes settings where transmission is optimal, but the usable field-of-view is reduced below 10″ to the indicated diameter (in arcseconds).

Start (Å)	End (Å)	Filter	CCD / Aperture	x1 (pix)	y1 (pix)	x2 (pix)	y2 (pix)	Max % Light Loss
3878	3881	FR418N18	PC1-FIX	402.3	225.0	402.3	225.0	2
4177	4182	FR418N	WF4-FIX	750.3	275.5	750.3	275.5	3
4182	4186	FR418P15	WF4-FIX	596.5	515.9	596.5	515.9	2
4571	4582	FR418P15	WF2-FIX	130.7	225.8	130.7	225.8	13
4582	4593	FR418N	WF3-FIX	713.7	125.6	713.7	125.6	13
4720	4733	FR418N	WF3-FIX	708.5	749.9	708.5	749.9	14
4733	4746	FR533N	WF3-FIX	689.3	748.9	689.3	748.9	14
4863	4873	FR533N	WF3-FIX	694.4	135.5	694.4	135.5	8
4873	4884	FR533P15	WF2-FIX	128.3	205.1	128.3	205.1	8
5176	5183	FR533P15	PC1-FIX	698.6	393.3	698.6	325.9	FOV~9"
5183	5188	FR533N	WF3-FIX	233.5	127.4	233.5	127.4	2
5335	5337	FR533P15	WF4-FIX	593.1	534.9	593.1	534.9	1
5337	5339	FR533N	WF4-FIX	750.9	294.7	750.9	294.7	1
5741	5743	FR533N33	WF3-FIX	370.8	126.5	370.8	126.5	1
6208	6221	FR680P15	WF2-FIX	124.9	213.6	124.9	213.6	8
6221	6238	FR680N	WF3-FIX	703.6	128.1	703.6	128.1	11
6584	6587	FR680N	WF3-FIX	242.6	127.0	242.6	127.0	1
6587	6590	FR680P15	PC1-FIX	699.1	294.3	699.1	315.3	FOV~9"
7241	7246	FR680N	WF4-FIX	748.3	285.6	748.3	285.6	2
7246	7251	FR680N	WF4-FIX	749.6	743.5	749.6	743.5	2
7600	7602	FR680N33	WF3-FIX	381.6	126.4	381.6	126.4	1
7602	7605	FR680N18	PC1-FIX	427.0	230.0	427.0	230.0	1
8072	8074	FR868N33	WF3-FIX	360.9	129.7	360.9	129.7	1
8074	8077	FR868N18	PC1-FIX	471.5	231.0	471.5	231.0	1
8910	8920	FR868N	WF3-FIX	223.4	125.3	223.4	125.3	2
8920	8945	FR868P15	PC1-FIX	701.1	339.1	701.1	467.5	FOV~7"
9456	9478	FR868P15	WF2-FIX	127.0	194.2	127.0	194.2	13
9478	9501	FR868N	WF3-FIX	684.3	135.4	684.3	135.4	13

3.4 Redshifted [OII] Quad Filters

The redshifted [OII] quad filter was designed to map onto a four-faceted WFC configuration. A partial SOFA wheel rotation of -33° is required to move filter quadrant 1 (3763Å) into WF2 and WF3, with some vignetting of both camera fields. The projections of the redshifted [OII] filter settings FQUVN and FQUVN33 onto the field-of-view are essentially identical to those of the POLQ and POLQN33 filters, respectively (Figure 3.6). The vignetted regions are similar, and the location of aperture FQUVN33 is identical to that of POLQN33.

The nominal and rotated filter wheel positions for the redshifted [OII] quad filter are each associated with different filter names. This allows pipeline calibration and database retrievals to proceed smoothly. The filter names are summarized in Table 3.9.

The required central wavelength is selected by filter name and aperture location. Filter element FQUVN (Filter Quad UltraViolet Narrow) has three possible apertures, each of which is nominally centered in one of the three WF channels and associated with a unique central wavelength. The filter element FQUVN33 corresponds to a single central wavelength. In addition to the filter name and aperture, a central wavelength is also requested in the proposal instructions in order to provide a consistency check. Aperture names are discussed further in section 3.9, “Apertures”, on page 60.

Table 3.9: Redshifted [OII] Quad Filter Elements.

Filter Name	Aperture Name	FOV Location	Quad	Mean Wavelength (Å)	Effective Width (Å)	Comments
FQUVN	WF2	WF2	D	3992	64	Nominal filter wheel position
FQUVN	WF3	WF3	C	3913	59	Nominal filter wheel position
FQUVN	WF4	WF4	B	3830	57	Nominal filter wheel position
FQUVN33	FQUVN33	WF2	A	3765	73	Filter rotated -33˚

3.5 Polarizer Quad Filter

The polarizer quads were also designed to map onto a four-faceted WFC configuration and, consequently, also require a partial filter rotation of -33˚ to move the filter quadrant 1 (nominal polarization angle 135˚) into WFCs 2 and 3, with some vignetting of both camera fields. Several additional partial rotations have been added to allow observations with different polarization angles on the same CCD.

The polarizer quad may be used in several ways: by observing the target with each camera, by observing the target with the same camera using different partial rotations of the polarizer quad, or by observing the target with the same camera using different roll angles of the spacecraft. The first method has the drawback that calibration is complicated by uncertainties in the relative photometric calibration between cameras, while the second method uses the same camera but has non-optimal polarization angles and limited fields of view. The third method may present scheduling difficulties due to constraints on the spacecraft roll angle, and the need to rotate undersampled images. (See Biretta and Sparks 1995, “WFPC2 Polarization Observations: Strategies, Apertures, and Calibration Plans,” WFPC2 Instrument Science Report 95-01.)

The polarizer is designed for problems where large polarization angles are observed, and is not suitable for problems requiring precision of order 3% or better. The required polarization angle is selected by filter name and aperture location. The transmission of the quad polarizer is shown in Figure 3.7. The

Table 3.10: Polarizer Quad Filter. Polarization angle 0° lies along +X direction in Figure 3.11

Filter Name	Aperture Name	FOV Location	Polarization Angle	Comments
POLQ	PC1	PC1	135°	Nominal filter wheel position
POLQ	WF2	WF2	0°	Nominal filter wheel position
POLQ	WF3	WF3	45°	Nominal filter wheel position
POLQ	WF4	WF4	90°	Nominal filter wheel position
POLQN33	POLQN33	WF2	102°	Filter wheel rotated -33°
POLQP15	POLQP15P	PC	15°	Filter wheel rotated +15°
POLQP15	POLQP15W	WF2	15°	Filter wheel rotated +15°
POLQN18	POLQN18	WF2	117°	Filter wheel rotated -18°

polarizer is afocal and must therefore usually be used with another filter which will largely define the shape of the passband.

Figure 3.6: Polarizer Quads. The schematics show the filter projected onto the field-of-view for all rotated positions. Apertures are marked. Dashed lines indicate the central region of each quad which is free of vignetting and cross-talk. Greyscale images are VISFLATs of the polarizer with F555W.

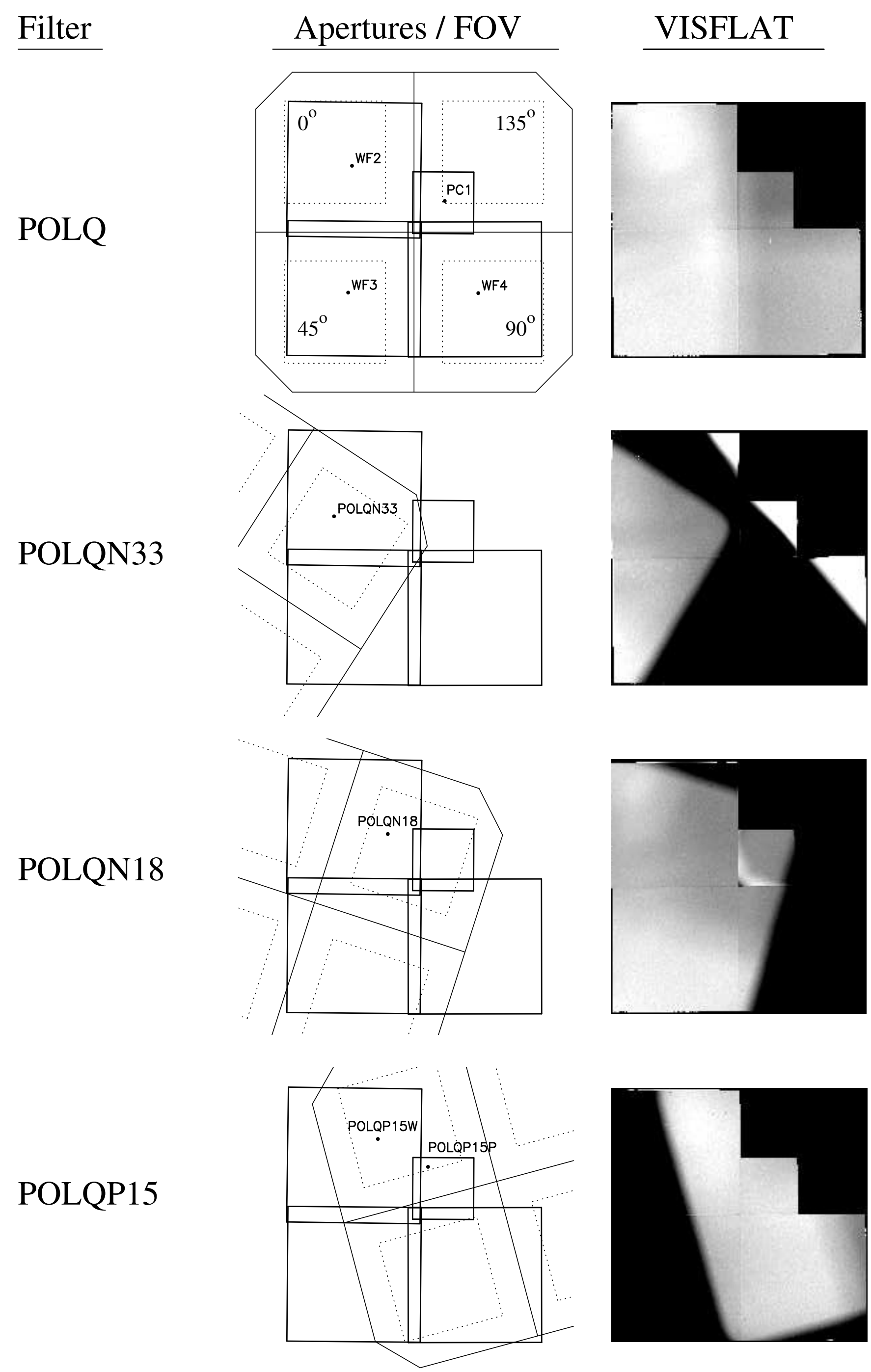

Figure 3.7: Polarizer Transmission for light polarized perpendicular (dotted curve) and parallel (solid curve) to the filter polarization direction.

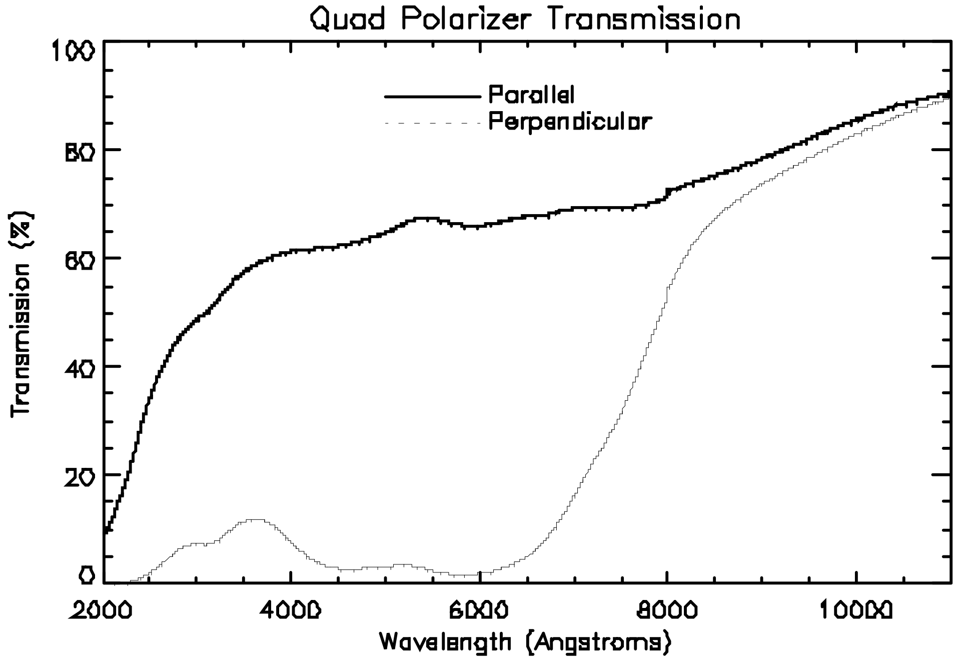

3.6 Methane Quad Filter

The methane band quad filter, known as the jewel-quad, was designed for a four-faceted WF/PC configuration to permit imaging with both four WFC CCDs and four PC CCDs. WFC imaging is recovered for the first quadrant element of the filter (6193Å) by a partial SOFA wheel rotation of -33° which moves quadrant 1 into WF2 and WF3 with some vignetting of both camera fields. PC imaging with all four elements of the methane band jewel-quad cannot be recovered, but partial SOFA wheel rotations of -15° and +15° are implemented to recover two of the four methane band filters (8929Å and 6193Å). The +15° rotation of the filter wheel, however, results in some vignetting of PC1's field-of-view. The filter projections associated with the methane band jewel-quad are shown in Figure 3.8. Each of the four filter wheel positions are associated with unique filter names, as summarized in Table 3.11 on page 54.

The required central wavelength is selected by filter name and aperture location. Filter element FQCH4N (Filter Quad Methane Narrow) has three possible apertures, each of which is located in one of the three WF channels and associated with a unique central wavelength, while FQCH4N33 is associated with one possible central wavelength. FQCH4N15 and FQCH4P15 are both associated with one central wavelength for PC1 observations. In addition to the filter name and aperture, a central wavelength is also requested in the proposal instructions in order to provide a consistency check.

Table 3.11: Methane Band Quad Filter. The filter and aperture names should be specified on the Phase II proposal as shown here.

Filter Name	Aperture Name	FOV Location	Quad	Mean Wavelength (Å)	Effective Width (Å)	Comments
FQCH4N	FQCH4W2	WF2	A	5433	38	Nominal filter position
FQCH4N	FQCH4W3	WF3	D	8929	64	Nominal filter position
FQCH4N	FQCH4W4	WF4	C	7274	51	Nominal filter position
FQCH4N33	FQCH4N33	WF2/WF3	B	6193	44	Filter rotated -33°
FQCH4N15	FQCH4N15	PC1	B	6193	44	Filter rotated -15°
FQCH4P15	FQCH4P15	PC1	D	8929	64	Filter rotated +15°

3.7 Wood's Filters

WFPC2 features two solar-blind Wood's filters, for FUV (<2000Å) imaging. It was shown by Wood in the 1930s (Physical Optics, 1934, R. W. Wood) that thin layers of alkali metals transmit FUV wavelengths while providing very efficient long wavelength blocking due to the plasma frequency of the free electrons. Wood's filters have been built for WFPC2 at JPL using thin (5000Å) layers of sodium sandwiched between two MgF_2 substrates. These Wood's filters have a broad bandpass from 1200Å to 2100Å with visible-light transmission lower than 10^{-8}. The best conventional UV filters exhibit visible-light transmission of 10^{-3} to 10^{-4}. Many astronomical objects emit 10^4 to 10^7 visible photons for every FUV photon. In such cases, a Wood's filter (or "solar blind" detector as on STIS) is essential for FUV imaging so that the visible light leak does not dominate the observation. The main problem experienced with Wood's filters is long term instability. Sodium is a very reactive metal, and attempts to passivate the sodium layer have met with limited success. It is possible that as the Wood's filters age pinholes will form which transmit visible light. This transmitted light will appear as an increase in the background level at the focal plane. No indications of any degradation on-orbit have been observed.

Figure 3.8: Methane Quad Filter. The mapping to the focal plane for nominal and rotated (-33º, -15º, and +15º) SOFA positions is shown. Dashed lines indicate the limits of the unvignetted field-of-view on each quad.

Filter — Apertures / FOV

FQCH4N

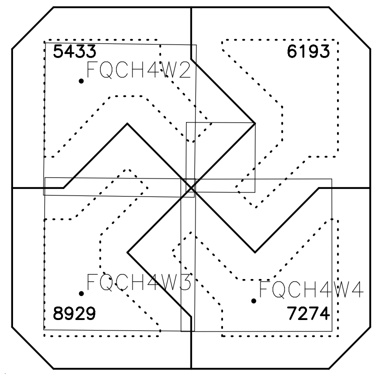

FQCH4N33

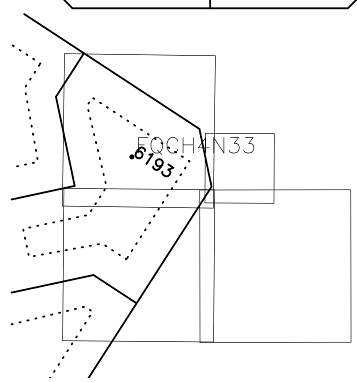

FQCH4N15

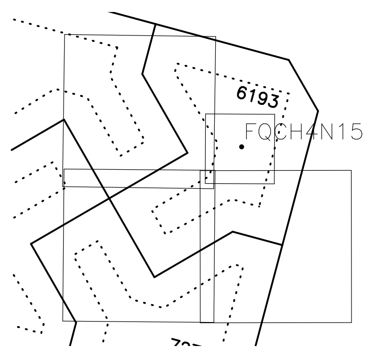

FQCH4P15

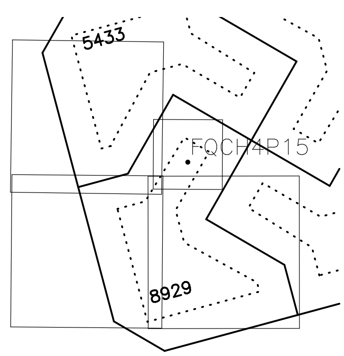

Figure 3.9: Wood's Filters. Greyscale flat field images show the field-of-view available with the two Wood's filter options F160BW and F160BN15.

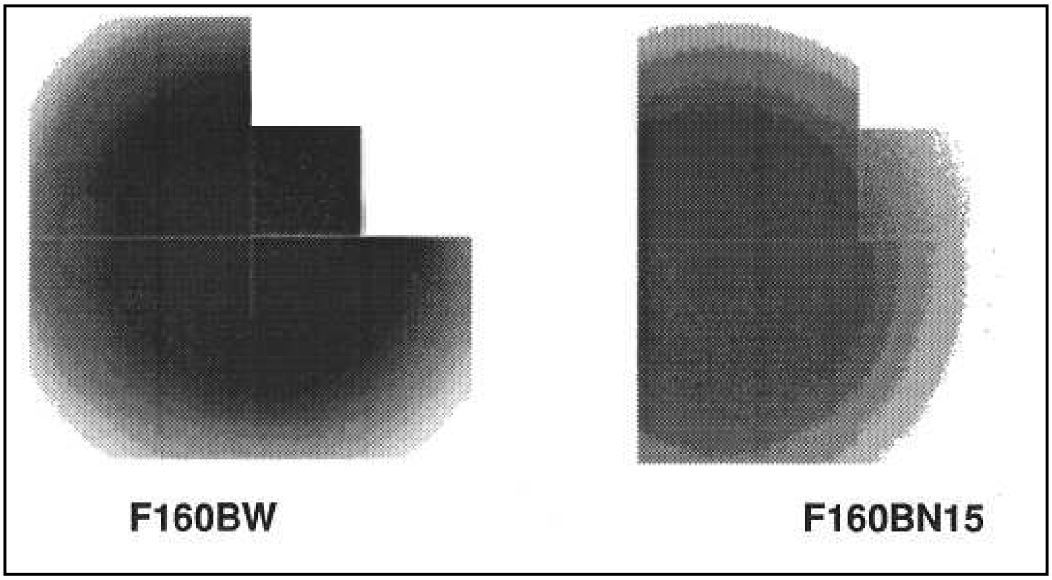

The Wood's filters can be used as a broadband filter, or in combination with the CaF_2 long-pass filter to suppress geocoronal emission, or, crossed with one of the other UV filters, such as the suprasil blocker F165LP, to define a solar-blind UV photometric system. As discussed at the beginning of this chapter, the image will be out of focus in the last case. WFPC2's Wood's filters are circular with a clear aperture of 41 mm. Two similar Wood's filters (F160AW and F160BW) were mounted in SOFA wheel 1 to provide some redundancy. In Thermal Vacuum testing F160AW showed evidence for pinholes, which cause excessive red leak in some parts of its field. Therefore the preferred filter for far UV imaging with minimal red leak in WFPC2 is F160BW.

In the nominal filter wheel position PC1 has a clear field-of-view but, there is significant vignetting in all three WFCs. A partial filter wheel rotation of -15° produces a larger field-of-view in WF3, although some vignetting remains. The options are illustrated in Figure 3.9. The imaging performance of the Wood's filters is continually monitored for signs of aging such as visible light leaks. Additional partial rotations could be implemented in the future, to position an unaffected region of the filter into a WF or PC1, if necessary. The unvignetted filter projections associated with the two planned filter positions are shown schematically in Figure 3.9. Each filter position is associated with a unique name as summarized in Table 3.12.

The filter name must be selected on the basis of whether a PC or WF3 observation is required.

Table 3.12: Wood's Filters. The filter and aperture names should be specified on the Phase II proposal as shown below.

Filter Name	Aperture Name	FOV Location	Mean Wavelength (Å)	Effective Width (Å)	Comments
F160BW	PC1	PC1	1600	900	Nominal filter position
F160BN15	F160BN15	WF3	1600	900	Filter rotated -15°

3.8 Red Leaks in UV Filters

The "red leaks" in the UV filters are shown in Figure 3.10 for F122M, F160BW (the new Wood's filter), F170W, F185W F218W F255W, F300W, and F336W. The presence of significant red leaks in the UV filters, together with the much greater sensitivity and wavelength coverage in the red part of the spectrum, makes calibration of UV observations difficult. Table 3.13 shows red leak estimates as a percentage of the total detected flux from de-reddened stellar sources, ordered by spectral type. In each column, the red leak is defined as the percentage of the detected flux longward of the cutoff wavelength in the second row. In the presence of interstellar reddening, the red leaks will be larger. Note that the SYNPHOT synthetic photometry package can be used to estimate the counts contributed by red leak for various particular situations, and for filters other than those plotted below.

There is significant variation of the UV throughput due to build-up of molecular contaminants on the CCD windows, and decontamination procedures used to remove this contamination. See "Time Dependence of UV Response" on page 137.

Figure 3.10: UV Filter Red Leaks. Includes the on-orbit measurements of system response.

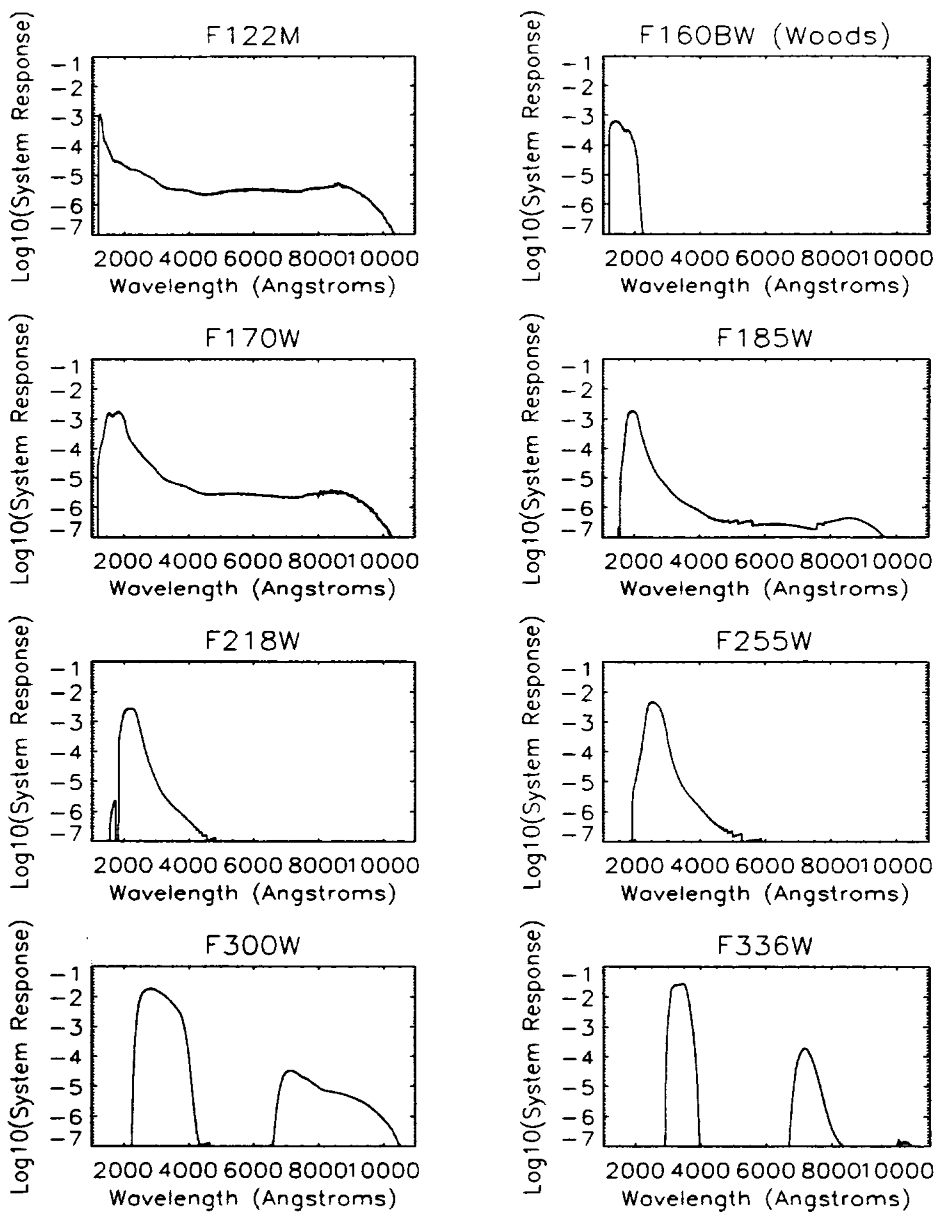

Table 3.13: Red Leak in UV Filters. A synthetic photometry calculation with de-reddened BPGS stellar spectra and system response from on-orbit data.

Filter		F122M	F160BW	F170W	F185W	F218W	F255W	F300W	F336W	F122M	F160B	F170W	F185W	F218W	F255W	F300W	F336W
Filter Central λ (nm)		122	160	170	185	218	255	300	336	122	W160	170	185	218	255	300	336
Cutoff λ (nm)		140	240	260	260	280	310	400	400	380	380	380	380	380	380	380	380
9SGR	O5	16.9		0.7	0.4	0.2	0.3		0.1	0.3		0.1				0.5	0.1
9 SGE	O8F	16.9		0.7	0.4	0.2	0.3		0.1	0.3		0.1				0.5	0.1
HR8D23	O6	21.8		1.0	0.5	0.3	0.4		0.1	0.6		0.1				0.6	0.1
-1935	B1V	20.1		0.8	0.4	0.3	0.4		0.1	0.6		0.1				0.6	0.2
60CYG	B1V	20.1		0.8	0.4	0.3	0.4		0.1	0.6		0.1				0.6	0.2
102 HER	B2V	22.5		1.2	0.6	0.4	0.4	0.1	0.1	1.1		0.2	0.1			0.8	0.2
ETAHYA	B3V	22.7		1.2	0.6	0.4	0.5	0.1	0.1	1.3		0.3	0.1			0.9	0.2
IOTA HER	B3V	22.7		1.2	0.6	0.4	0.5	0.1	0.2	1.3		0.3	0.1			0.9	0.2
HR 7899	B4V	22.7		1.2	0.6	0.4	0.5	0.1	0.2	1.4		0.3	0.1			0.9	0.2
38OPH	A1V	30.0		1.6	0.7	0.5	0.5	0.1	0.2	2.9		0.5	0.1			1.1	0.3
HR7174	B6V	30.7		1.8	0.8	0.5	0.5	0.1	0.3	3.8		0.7	0.2		0.1	1.3	0.4
9 VUL	B7V	30.8		1.8	0.8	0.5	0.5	0.1	0.3	3.9		0.7	0.2		0.1	1.4	0.4
HD 189689	B9V	41.1		2.4	0.9	0.5	0.6	0.2	0.3	7.4		1.0	0.2		0.1	1.6	0.4
THETA VIR	A0V	59.6		4.0	1.2	0.6	0.8	0.3	0.6	20.3		2.2	0.4	0.1	0.1	2.5	0.7
NUCAP	B9V	58.6		3.7	1.2	0.6	0.8	0.3	0.5	18.3		2.0	0.4	0.1	0.1	2.2	0.6
HR6169	A2V	59.5		4.0	1.2	0.6	0.8	0.3	0.6	20.1		2.2	0.4	0.1	0.1	2.3	0.7
HD140849A	A1V	73.7		3.8	1.1	0.6	0.7	0.3	0.5	23.7		2.0	0.4	0.1	0.1	2.0	0.6
69HER	A2V	59.5		3.9	1.2	0.6	0.8	0.3	0.6	20.0		2.2	0.4	0.1	0.1	2.2	0.7
HD140849B	A3V	89.0		6.5	1.5	0.8	1.0	0.4	0.6	44.0		3.9	0.6	0.1	0.2	2.4	0.7
58AQL	A0V	75.5		4.3	1.3	0.6	0.8	0.3	0.7	28.6		2.5	0.5	0.1	0.1	2.7	0.8
78HER	B9V	75.0		4.2	1.2	0.6	0.7	0.3	0.7	27.5		2.4	0.5	0.1	0.1	2.4	0.8
HR6570	A7V	89.7		7.0	1.6	0.8	1.0	0.4	0.7	47.6		4.4	0.7	0.1	0.2	2.6	0.9
HD187754	A2V	97.9		11.0	2.1	0.9	1.2	0.5	0.9	64.4		7.4	1.0	0.2	0.2	3.2	1.1
THETA1SER	A5V	97.7		9.8	1.9	0.9	1.1	0.4	0.8	60.3		6.2	0.8	0.1	0.2	2.6	0.9
PRAESEPE 276		99.7		12.1	2.2	1.0	1.2	0.5	0.9	67.5		8.1	1.1	0.2	0.2	2.9	1.0
PRAESEPE114		99.7		11.6	2.2	1.0	1.2	0.5	0.9	66.0		7.6	1.0	0.2	0.2	2.7	1.0
PRAESEPE154		100.0		17.0	3.0	1.1	1.3	0.5	0.9	71.9		11.4	1.4	0.2	0.2	2.8	1.0
HD140192	A5V	100.0		17.4	3.0	1.1	1.3	0.6	0.9	72.7		11.7	1.5	0.2	0.2	2.9	1.1
PRAESEPE226		100.0		17.2	3.0	1.1	1.3	0.6	1.0	72.7		11.6	1.4	0.2	0.2	2.7	1.1
PRAESEPE37		100.0		38.8	7.7	2.0	1.7	0.6	1.0	80.8		27.0	3.9	0.3	0.3	2.8	1.1
HD191177	F4V	100.0		64.9	17.6	3.0	2.3	0.8	1.1	86.1		48.4	10.1	0.6	0.5	3.6	1.3
PRAESEPE332		100.0		62.4	16.3	2.9	2.2	0.7	1.0	84.6		44.9	8.8	0.5	0.4	2.9	1.1
BD+293891	F6V	100.0		67.4	19.4	3.7	2.5	0.8	1.1	86.4		49.8	11.0	0.7	0.4	3.1	1.2
PRAESEPE222		100.0		50.7	11.4	2.8	2.2	0.8	1.1	84.7		36.8	6.2	0.5	0.4	2.8	1.2
HD35246	F8V	100.0		52.1	11.8	2.9	2.2	0.8	1.3	85.8		38.6	6.6	0.5	0.4	2.8	1.4
BD+263780	G0V	100.0		52.4	11.9	2.9	2.2	0.9	1.3	86.0		38.9	6.7	0.5	0.4	2.8	1.4
HD 148816	F9V	100.0		51.1	11.5	2.8	2.2	0.8	1.2	85.0		37.2	6.3	0.5	0.3	2.8	1.3
HD155675	F8V	100.0		69.0	20.5	4.7	3.4	1.0	1.3	88.7		53.3	12.4	0.9	0.6	3.3	1.4
PRAESEPE 418		100.0		70.2	21.1	4.8	3.5	1.0	1.4	89.4		55.0	13.2	1.0	0.6	3.2	1.5
HYAD 1		100.0		71.4	21.9	4.8	3.5	1.1	1.5	90.0		56.8	14.1	1.0	0.6	3.4	1.6
HD 122693	F8V	100.0		71.6	22.1	4.9	3.5	1.1	1.6	90.1		57.1	14.2	1.1	0.6	3.5	1.7
HD 154417	F8V	100.0		70.6	21.4	4.8	3.5	1.1	1.4	89.5		55.5	13.4	1.0	0.6	3.2	1.5
HYAD 2		100.0		89.2	46.7	7.9	3.4	1.2	1.6	91.2		71.6	30.3	1.7	0.6	3.3	1.7
HD 227547	G5V	100.0		89.5	47.2	8.0	3.4	1.2	1.7	91.4		72.0	30.7	1.7	0.6	3.3	1.8
HD 154760	G2V	100.0		89.3	46.8	7.9	3.4	1.2	1.6	91.3		71.6	30.3	1.7	0.6	3.3	1.7
HD 140605	G2V	100.0		89.9	48.2	8.1	3.5	1.3	1.8	91.8		73.2	32.0	1.8	0.7	3.4	1.9
HYAD 15		100.0		90.1	48.5	8.0	3.5	1.3	1.8	92.1		73.7	32.5	1.8	0.7	3.4	1.9
HD 139777A	K0V	100.0		89.8	47.7	8.0	3.4	1.3	1.8	91.7		72.8	31.5	1.7	0.6	3.5	1.9
HD 136274	G8V	100.0		91.4	51.6	8.3	3.5	1.7	2.3	93.4		77.1	36.6	2.0	0.7	3.6	2.4
HYAD26		100.0		91.6	52.3	8.3	3.6	1.7	2.3	93.5		77.6	37.3	2.1	0.7	3.6	2.4
HD 150205	G5V	100.0		91.7	52.3	8.4	3.6	1.7	2.4	93.5		77.6	37.4	2.1	0.8	3.8	2.4
HYAD 21		100.0		92.8	55.7	8.6	3.7	2.1	2.8	94.6		80.7	41.8	2.4	0.8	3.9	2.9
+02 3001	G8V	100.0		93.0	56.1	8.6	3.6	2.2	3.1	94.8		81.1	42.3	2.4	0.8	4.3	3.2
HD190571	G8V	100.0	0.3	99.5	95.2	40.0	11.3	3.4	3.6	96.7	0.1	91.4	80.4	16.0	3.0	6.1	3.7
HYAD183		100.0	0.3	99.6	96.0	41.6	11.7	4.3	4.6	97.5	0.1	93.1	83.8	18.3	3.4	6.7	4.7
HD140470	K3V	100.0	0.3	99.6	96.2	42.2	11.9	4.5	4.8	97.5	0.1	93.3	84.4	19.0	3.5	7.0	4.9
HD154712	K4V	100.0	0.2	99.7	95.7	45.7	15.8	6.6	6.7	98.3	0.1	95.3	87.4	24.6	5.4	9.4	6.8
HYAD185		100.0	0.2	99.7	96.7	50.0	15.7	8.0	7.9	98.6	0.1	96.0	89.5	28.6	5.5	10.6	8.0
+382457	K8V	100.0	0.2	99.7	96.6	48.6	16.5	8.8	9.1	98.7	0.1	96.4	90.1	28.7	6.3	11.5	9.1
HYAD173		100.0	0.1	99.5	93.8	32.0	8.5	11.8	12.8	99.0		96.9	88.7	19.8	3.8	14.3	12.9
GL40	M0V	100.0	0.1	99.6	94.9	34.5	8.8	14.5	15.4	99.2		97.5	90.7	22.8	4.2	17.4	15.5
HYAD 189		100.0	0.1	99.6	95.3	35.8	9.1	15.7	16.8	99.3		97.7	91.5	24.3	4.4	18.4	16.9
HD 151288	K7V	100.0	0.1	99.7	95.6	37.0	9.4	16.5	17.4	99.3		97.8	91.9	25.5	4.7	19.3	17.4
HD157881	K7V	100.0	0.1	99.7	95.6	36.6	9.2	16.7	17.6	99.3		97.8	91.9	25.2	4.5	19.4	17.7
HD1326d3	M0V	100.0	0.1	99.7	95.8	37.5	9.4	17.7	18.9	99.4		97.9	92.3	26.2	4.7	20.5	18.9
GL15A	M0V	100.0	0.1	99.8	97.7	48.6	11.5	27.3	26.7	99.6	0.1	98.8	95.6	38.8	6.7	30.4	26.8
GL49	M2V	100.0	0.1	99.8	97.3	45.8	10.7	25.5	25.0	99.6	0.1	98.7	95.1	35.9	6.0	28.7	25.1
GL1D9	M4V	100.0	0.1	99.9	98.2	54.5	12.5	34.1	32.2	99.7	0.1	99.1	96.7	46.1	7.9	37.2	32.3
GL15B	M6V	100.0	0.2	99.9	99.2	69.7	17.7	51.1	46.0	99.9	0.1	99.6	98.4	64.0	13.3	53.5	46.1
GL83.1	M8V	100.0	0.1	99.7	95.9	38.2	8.9	17.4	15.5	99.4		97.9	92.4	26.8	3.9	20.1	15.5
GL65	M5V	100.0	0.1	99.8	97.0	43.3	9.2	22.4	17.8	99.6		98.5	94.4	33.0	4.3	25.2	17.9

3.9 Apertures

The WFPC2 camera configuration and filter set require a substantial number of apertures for full utilization of its capabilities. All possible aperture and filter combinations are given in Table 3.14.

Each camera has an associated 'optimum' aperture close to the geometric center of its field-of-view (FOV). These positions have been adjusted to reflect CCD performance following SMOV and to allow for pyramid vignetting. The aperture designations are WF2, WF3, WF4, and PC1 for the individual cameras and WFALL for the three-WFC combination. WFALL is located close to the apex in WF3 (see Figure 3.11). Observers are expected to place small or unresolved targets on these apertures. Note that normally all four CCDs are read out even if a specific CCD is selected with an aperture. This is discussed in section 2.8, "CCD Orientation and Readout", on page 31.

In cases where the observer does not want to use the current 'optimum' centers, a complimentary set of apertures has been implemented specifically for this purpose. These locations remain fixed and correspond roughly to the geometric center of each camera's field-of-view. They are designated WF2-FIX, WF3-FIX, WF4-FIX, PC1-FIX, and WFALL-FIX. Observers are expected to place extended targets on these apertures.

An additional set of aperture names have been defined for use with the WFPC2 filters which require partial rotations. The characteristics and uses of these filters are discussed earlier in this Chapter. In the nominal filter position, the three WFC segments of the [OII], Methane and Polarizer quad filters can be selected with an aperture for each camera corresponding to the optimum or geometric camera centers. The partially rotated quad filters, which generally fall into more than one camera, have been assigned apertures in the camera which provides the largest clear aperture. The pixel coordinates of these apertures will be reviewed on a regular basis to reflect changes in CCD and filter cosmetics. There are no analogous fixed apertures for the partially rotated filter configurations. The aperture name is generally the same as the (rotated) filter name. For the Wood's filters, the nominal filter position is used for the PC1 FOV only, while the rotated filter position is used for WFC observations. The linear ramp filters are unique because the ultimate location of the target will be determined from the central wavelength specified and so an aperture name is not required.

Occasionally the V2-V3 coordinates of the WFPC2 apertures are updated to correct slow drifts of the HST focal plane relative to the spacecraft (V1, V2, V3) system. Table 3.15 shows this history. The previous V2-V3 coordinates for any aperture can be derived by setting ($V2_2$,$V3_2$) to the values in Table 3.14, and then computing the earlier coordinates.

Table 3.14: Aperture Definitions. The pixel coordinate system uses pixel numbers (row, column) for the CCD in use. See Figure 3.11: on page 62 or Figure 1.1: on page 2 for the definition of the V2-V3 coordinate system.

Aperture Name	Filter Name	CCD	Location	CCD Pixel X	CCD Pixel Y	Coordinates[a] V2	Coordinates[a] V3
PC1		PC	Optimum center PC	420	424.5	2.160	-30.490
WF2		WF2	Optimum center WF2	423.5	414	-51.530	-5.920
WF3		WF3	Optimum center WF3	436[b]	424.5[b]	-0.150	48.470
WF4		WF4	Optimum center WF4	423	421	54.830	-6.320
WFALL		WF3	Optimum near apex	133[c]	149[c]	2.020	7.920
PC1-FIX		PC	Fixed center PC	420	424.5	1.810	-30.900
WF2-FIX		WF2	Fixed center WF2	423.5	414	-51.530	-5.920
WF3-FIX		WF3	Fixed center WF3	416.5	424.5	1.230	47.100
WF4-FIX		WF4	Fixed center WF4	423	421	54.830	-6.320
WFALL-FIX		WF3	Fixed near apex	133[c]	149[c]	2.020	7.920
FQUVN33	FQUVN33	WF2	Optimum for FOV	292	520	-49.924	10.802
POLQN33	POLQN33	WF2	Optimum for FOV	292	520	-49.924	10.802
POLQN18	POLQN18	WF2	Optimum for FOV	380[d]	200[d]	-33.280	-17.717
POLQP15P	POLQP15	PC	Optimum for FOV	200	680	-13.057	-31.643
POLQP15W	POLQP15	WF2	Optimum for FOV	500	260	-45.892	-22.069
FQCH4NW2	FQCH4N	WF2	Optimum for FOV	602	608	-77.669	-5.102
FQCH4NW3	FQCH4N	WF3	Optimum for FOV	602	608	0.928	72.995
FQCH4NW4	FQCH4N	WF4	Optimum for FOV	640	386	67.687	11.323
FQCH4N33	FQCH4N33	WF2	Optimum for FOV	264	436	-41.997	6.950
FQCH4N15	FQCH4N15	PC	Optimum for FOV	420	424.5	2.164	-30.494
FQCH4P15	FQCH4P15	PC	Optimum for FOV	400	312	5.129	-26.221
F160BN15	F160BN15	WF3	Optimum for FOV	436	424.5	-0.153	48.470

a. V2-V3 coordinates in effect after 1996 day 127 (May 6). CCD pixel positions unchanged.
b. CCD pixel position in effect after 1994 day 101 (April 11).
c. WFALL and WFALL-FIX "meta-chip" coordinates are (903,904).
d. CCD pixel position in effect after 1995 day 86 (March 27).

Table 3.15: Updates to (V2,V3) Positions of WFPC2 Apertures.

Date in Effect	V2	V3	Rotation
1994 day 101 - 1996 day 105	$V2_0$	$V3_0$	PA_0
1996 day 105 - 1996 day 127	$V2_1 = V2_0 - 0.12''$	$V3_1 = V3_0 + 0.11''$	$PA_1 = PA_0 + 0.14^\circ$
>1996 day 127	$V2_2 = V2_0 + 0.46''$	$V3_2 = V3_0 + 0.39''$	$PA_2 = PA_0 + 0.14^\circ$

Figure 3.11: Precise CCD Alignments and Primary Aperture Locations. “FIX” apertures are in the same locations, unless otherwise indicated. Dashed lines show vignetted region along CCD boundaries. Short lines and “X”s in outer corners indicate directions of CCD bloom and OTA diffraction spikes, respectively. Origin of the (V2, V3) system is at the origin of the plot axes, with V2, V3, and U3 exactly along diagonal lines as marked. (V2,V3) system is post-1996 day 127. CCDs have pixel (1,1) located where the four CCDs overlap.